

**RADC-TR-89-213**  
**Final Technical Report**  
**October 1989**



# **ELECTROOPTICAL QUANTUM WELLS**

**Martin Marietta Laboratories**

**Richard P. Leavitt, John W. Little, K.J. Ritter**

**AD-A226 102**

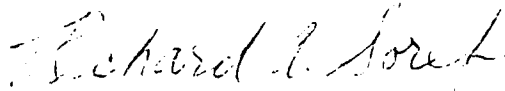
*APPROVED FOR PUBLIC RELEASE; DISTRIBUTION UNLIMITED.*

**ROME AIR DEVELOPMENT CENTER**  
**Air Force Systems Command**  
**Griffiss Air Force Base, NY 13441-5700**

This report has been reviewed by the RADC Public Affairs Division (PA) and is releasable to the National Technical Information Service (NTIS). At NTIS it will be releasable to the general public, including foreign nations.

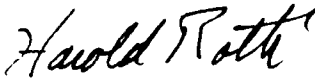
RADC-TR-89-213 has been reviewed and is approved for publication.

APPROVED:



RICHARD A. SOREF  
Project Engineer

APPROVED:



HAROLD ROTH  
Director of Solid State Sciences

FOR THE COMMANDER:



JAMES W. HYDE III  
Directorate of Plans & Programs

If your address has changed or if you wish to be removed from the RADC mailing list, or if the addressee is no longer employed by your organization, please notify RADC (ESOC) Hanscom AFB MA 01731-5000. This will assist us in maintaining a current mailing list.

Do not return copies of this report unless contractual obligations or notices on a specific document require that it be returned.

UNCLASSIFIED

SECURITY CLASSIFICATION OF THIS PAGE

REPORT DOCUMENTATION PAGE				Form Approved OMB No. 0704-0188		
1a. REPORT SECURITY CLASSIFICATION UNCLASSIFIED			1b. RESTRICTIVE MARKINGS N/A			
2a. SECURITY CLASSIFICATION AUTHORITY N/A			3. DISTRIBUTION/AVAILABILITY OF REPORT Approved for public release; distribution unlimited.			
2b. DECLASSIFICATION/DOWNGRADING SCHEDULE N/A						
4. PERFORMING ORGANIZATION REPORT NUMBER(S)  N/A			5. MONITORING ORGANIZATION REPORT NUMBER(S)  RADC-TR-89-213			
6a. NAME OF PERFORMING ORGANIZATION  Martin Marietta Laboratories		6b. OFFICE SYMBOL (if applicable)	7a. NAME OF MONITORING ORGANIZATION  Rome Air Development Center (ESOC)			
6c. ADDRESS (City, State, and ZIP Code)  1450 South Rolling Road Baltimore MD 21227-3898			7b. ADDRESS (City, State, and ZIP Code)  Hanscom AFB MA 01731-5000			
8a. NAME OF FUNDING/SPONSORING ORGANIZATION  Rome Air Development Center		8b. OFFICE SYMBOL (if applicable)  ESOC	9. PROCUREMENT INSTRUMENT IDENTIFICATION NUMBER  F19628-86-C-0059			
8c. ADDRESS (City, State, and ZIP Code)  Hanscom AFB MA 01731-5000			10. SOURCE OF FUNDING NUMBERS			
			PROGRAM ELEMENT NO	PROJECT NO	TASK NO	WORK UNIT ACCESSION NO
			62702F	4600	19	59
11. TITLE (Include Security Classification)  ELECTROOPTICAL QUANTUM WELLS						
12. PERSONAL AUTHOR(S) Richard P. Leavitt, John W. Little, K.J. Ritter						
13a. TYPE OF REPORT Final		13b. TIME COVERED FROM <u>Mar 87</u> TO <u>Oct 88</u>		14. DATE OF REPORT (Year, Month, Day) October 1989		
15. PAGE COUNT 92						
16. SUPPLEMENTARY NOTATION  N/A						
17. COSATI CODES			18. SUBJECT TERMS (Continue on reverse if necessary and identify by block number)			
FIELD	GROUP	SUB-GROUP				
20	12		InGaAs/InAlAs Optical Modulation			
20	06	01	Quantum Wells Optical Waveguides			
			GaAs/AlGaAs Electro-optics			
19. ABSTRACT (Continue on reverse if necessary and identify by block number)  A detailed study of electro-refraction and electro-absorption in a new semiconductor quantum well system known as an asymmetric coupled quantum well is presented in this report. Resonant coupling of electron levels in a closely-spaced pair of quantum wells is shown to modify the exciton absorption spectrum and, through the Kramers-Kronig relation, lead to substantial changes in the index of refraction of single mode waveguides at wavelengths much longer than the absorption edge of the guide. Intensity and phase modulators have been fabricated and tested using GaAs/AlGaAs quantum wells (for operation at 0.86-0.95 $\mu\text{m}$ ) and InGaAs/InAlAs wells lattice-matched to InP substrates for use at 1.55 $\mu\text{m}$ .						
20. DISTRIBUTION/AVAILABILITY OF ABSTRACT <input checked="" type="checkbox"/> UNCLASSIFIED/UNLIMITED <input type="checkbox"/> SAME AS RPT <input type="checkbox"/> DTIC USERS			21. ABSTRACT SECURITY CLASSIFICATION UNCLASSIFIED			
22a. NAME OF RESPONSIBLE INDIVIDUAL Richard A. Soref			22b. TELEPHONE (Include Area Code) (617) 377-2380		22c. OFFICE SYMBOL RADC (ESOC)	

DD Form 1473, JUN 86

Previous editions are obsolete.

SECURITY CLASSIFICATION OF THIS PAGE  
UNCLASSIFIED

## TABLE OF CONTENTS

	Page
LIST OF FIGURES	ii
EXECUTIVE SUMMARY	v
I. INTRODUCTION	1
II. FIRST CONTRACT YEAR	3
A. BACKGROUND AND THEORY	3
B. EXPERIMENT	5
III. RESULTS FOR GaAs/AlGaAs STRUCTURES	9
A. IMPLICATIONS OF LOW-TEMPERATURE PHOTOCURRENT MEASUREMENTS	9
B. OBSERVATION OF COUPLING EFFECTS IN GaAs/AlGaAs ACQW STRUCTURES	18
C. ELECTRO-ABSORPTION AND ELECTRO-REFRACTION IN GaAs/AlGaAs ACQW WAVEGUIDES	25
IV. RESULTS FOR InGaAs/InAlAs STRUCTURES	38
A. GROWTH OF InGaAs/InAlAs ON InP SUBSTRATES	38
B. PHOTOCURRENT STUDIES OF InGaAs/InAlAs ACQW SAMPLES	43
C. ELECTRO-ABSORPTION AND ELECTRO-REFRACTION IN InGaAs/InAlAs ACQW WAVEGUIDES	55
V. DISCUSSION AND CONCLUSIONS	65
A. SUMMARY OF THE CONTRACT RESULTS	65
B. ADVANTAGES OF COUPLED QUANTUM WELLS	67
C. DESIGN OF OPTIMIZED ACQW STRUCTURES	68
D. RECOMMENDATIONS FOR FURTHER STUDY	70
ACKNOWLEDGMENTS	72
REFERENCES	74
APPENDIX A. DESCRIPTION OF SAMPLES	78
APPENDIX B. EXTERNAL PUBLICATIONS AND PRESENTATIONS RESULTING FROM THE CONTRACT	79

## LIST OF FIGURES

	Page
FIG. 1. Schematic diagram of the asymmetric coupled-quantum-well (ACQW) structure.	4
FIG. 2. Micrograph of a 250- $\mu\text{m}$ -diameter mesa diode processed for transmission measurements by removing the GaAs substrate.	7
FIG. 3. Bias-dependent, 8-K photoluminescence (PL) spectra from a p-i-n diode (sample 802) containing the ACQW structure with 8.8-nm-thick wide wells and thick (9.0-nm) barriers.	12
FIG. 4. Bias-dependent, 8-K photocurrent spectra from sample 802.	13
FIG. 5. Measured and calculated energies of the $h_1e_1$ transition as a function of applied bias for sample 802.	15
FIG. 6. Measured and calculated energies of the $h_1e_1$ transition as a function of applied bias for sample 800.	17
FIG. 7. Transmission electron micrograph of the ACQW region of sample 1121.	20
FIG. 8. 8-K photocurrent spectra of the GaAs/AlGaAs ACQW sample (sample 1121).	21
FIG. 9. Observed and calculated peak transition energies as functions of applied reverse bias in sample 1121.	23
FIG. 10. Calculated energies of the $l_1e_1$ and $l_1e_2$ transitions in an ACQW structure (sample 919) with 8.5-nm and 4.3-nm GaAs wells coupled by a 2.1-nm AlGaAs barrier.	27
FIG. 11. Interferograms measured in the Mach-Zehnder interferometer with 860-nm-wavelength light.	29
FIG. 12. Measured phase shift and intensity change in sample 919 at four different TM-polarized laser wavelengths.	31

FIG. 13. Measured change in the real and imaginary part of the effective waveguide refractive index in sample 919 at four different TM-polarized laser wavelengths.	32
FIG. 14. Calculated change in the real part of the refractive index for sample 919 as a function of electric field.	36
FIG. 15. Current-voltage (I-V) characteristic for an InGaAs p-i-n diode grown on InP.	42
FIG. 16. Current-voltage (I-V) characteristic for an InAlAs p-i-n diode grown on InP.	44
FIG. 17. Single-crystal x-ray diffraction spectrum of an InGaAs/InAlAs ACQW sample (EO-72) in the vicinity of the [004] InP substrate reflection.	46
FIG. 18. Room-temperature photocurrent spectra of a control sample (sample EO-64) containing 40 periods of 7.5-nm InGaAs quantum wells separated by 10.0-nm InAlAs barriers.	49
FIG. 19. Room-temperature photocurrent spectra of an ACQW sample (EO-72) containing 29 periods of 7.5- and 5.0-nm InGaAs quantum wells coupled by a 1.5-nm InAlAs barrier.	50
FIG. 20. Low-temperature (8 K) photocurrent spectra of sample EO-72 for several values of reverse bias.	51
FIG. 21. Calculated and observed (at 8 K) transition energies as functions of applied reverse bias for sample EO-72.	53
FIG. 22. Room-temperature photocurrent spectra of an InGaAs/InAlAs MQW waveguide sample (EO-77) containing only uncoupled 7.5-nm quantum wells.	58
FIG. 23. Room-temperature photocurrent spectra of an InGaAs/InAlAs MQW waveguide sample (EO-75) containing 7.5- and 5.0-nm quantum wells coupled by a 1.6-nm barrier.	59

FIG. 24. Phase shift and relative transmission measured as a function of reverse bias in 250- $\mu\text{m}$ -long waveguides containing uncoupled wells (sample EO-77) and asymmetric coupled wells (sample EO-75) of InGaAs/InAlAs. 61

FIG. 25. Changes in the real and imaginary parts of the effective waveguide refractive index as a function of reverse bias at 1.523  $\mu\text{m}$  in TM polarization in 250- $\mu\text{m}$ -long waveguides containing uncoupled wells (sample EO-77) and asymmetric coupled wells (sample EO-75) of InGaAs/InAlAs. 62

FIG. 26. Calculated changes in the real part of the MQW refractive index for the uncoupled and ACQW waveguides. 64

## EXECUTIVE SUMMARY

We present the results of a two-year contract to develop an optical phase shifter for use at 1.55  $\mu\text{m}$  based on the coupling of electron energy levels in a new type of quantum well system known as an asymmetric coupled quantum well (ACQW). The work was divided into two phases; in phase 1 we concentrated on studying the optical properties of the new quantum well system as grown in the GaAs/AlGaAs semiconductor system (for which there is a great deal of information in the scientific literature), and in phase 2 we established the growth techniques necessary to obtain high-quality InGaAs/InAlAs grown on InP substrates in order to extend the operating wavelength into the 1.55- $\mu\text{m}$  region.

An interim report described the results of the first year of work in detail, and a summary is given in this report. During the second year (with extension into a third year due to a redistribution of funding from RADC/Hanscom), we observed unambiguous evidence of the effects of coupling on the optical properties of GaAs/AlGaAs ACQWs (using photocurrent spectroscopy) and demonstrated substantial electro-absorption and electro-refraction effects (in GaAs/AlGaAs single-mode waveguides) resulting from an inter-well transition unique to the coupled system. Although this transition was not originally predicted as the phase-shifting mechanism in the ACQW system, it was found to dominate the below-band-gap optical properties under certain bias conditions. The results obtained with the GaAs/AlGaAs system were used to design an optimized device for use in the InGaAs/InAlAs system (lattice-matched to InP substrates) that is appropriate for 1.55- $\mu\text{m}$  operation. This materials system is much more difficult to grow with high optical quality than the GaAs/AlGaAs system. The design optimization proved valuable in reducing the number of growth iterations necessary to obtain usable devices.



Using group-III-composition calibrations based on x-ray diffraction measurements of semiconductor superlattices, we were able to grow very high-quality InGaAs/InAlAs quantum wells that showed strong coupling effects even at room temperature. Experimental comparisons at 1.523  $\mu\text{m}$  showed that the inter-well transition in the ACQW resulted in substantial enhancement (at a certain biases) in both the electro-refraction and the electro-absorption over that obtained for uncoupled wells. At this wavelength, the ACQW waveguides performed very well as intensity modulators giving large modulation depths with relatively low phase shifts. The results of measurements made at several wavelengths in the GaAs/AlGaAs system indicate that the ACQW waveguides will perform well as phase shifters at longer wavelengths (1.55  $\mu\text{m}$  or beyond). The extra degrees of freedom afforded by the ACQW (e.g. in the choice of absolute and relative well widths) should result in a number of new devices which exhibit superior performance to those based on the standard rectangular quantum well system.

## I. INTRODUCTION

This report summarizes the results of a two-year contract to develop an optical phase shifter for use at a wavelength of 1.55  $\mu\text{m}$  based on electro-refraction in InGaAs/InAlAs asymmetric coupled-quantum-well (ACQW) structures. In these structures, coupling of the electron subbands associated with the two wells leads to an avoided crossing of the electron subbands and delocalization of the corresponding wave functions. The dependence of the optical transition energies on electric field is modified by this coupling; because of the Kramers-Kronig relation between absorption and refraction, the refractive index changes as well. Thus the ACQW system exhibits both electro-absorptive and electro-refractive effects that are different from (and under many circumstances much larger than) corresponding effects that are known<sup>1,2</sup> to occur in uncoupled multiple-quantum-well (MQW) structures. When used in a single-mode waveguide configuration, the ACQW system can provide either a low-loss optical phase shift (for light with energy well below the exciton absorption energy) or an intensity modulation (for light with energy just below the exciton absorption energy).

The first phase of the program involved investigations of the electro-optic properties of GaAs/AlGaAs coupled quantum wells. This semiconductor system was used to identify the fundamental mechanisms contributing to the electro-optic properties of the ACQW system and to verify the predictions of sophisticated theoretical models. Many of the results obtained in the first phase are of intrinsic interest from the device point of view. The optical properties of GaAs/AlGaAs ACQW waveguides were investigated as a function of light wavelength, since a tunable dye laser was available to us for the contract.

The second phase of the program involved extending the results obtained with GaAs/AlGaAs quantum wells to the InGaAs/InAlAs material system (lattice matched to InP substrates). Optical intensity/phase modulators were fabricated from several ACQW waveguide samples grown with these materials; results of measurements using a 1.523- $\mu$ m He-Ne laser are described in detail below. Fuller characterization of these devices with a tunable infrared laser would be of interest.

In our interim report, written at the half-way point of the contract,<sup>3</sup> preliminary results on GaAs/AlGaAs ACQW growth and characterization were described. In Section II of this report, we shall briefly summarize those results to set the stage for what follows. Sections III and IV are devoted to the two primary tasks mentioned above: GaAs/AlGaAs and InGaAs/InAlAs devices, respectively. For each of these materials systems, we describe, in turn, the measurements of the basic optical properties of the quantum wells (based primarily on room- and low-temperature photocurrent spectroscopy) and the results of optical intensity and phase measurements performed as functions of sample bias and (in the case of the GaAs/AlGaAs devices) wavelength. In contrast to our interim report, we do not have a separate theory section; rather, theoretical results are integrated with the rest of the text where appropriate. Finally, Section V gives a summary of the status of ACQW modulators and suggests follow-up studies to clarify some of the issues raised during the contract.

To avoid repeating the details of samples grown for this contract, we provide an identifying sample number together with a full description of the structure for each quantum-well sample in Appendix A. In the main text, each sample is described the first time it is discussed; thenceforth, each sample is identified only by sample number. The samples that will be delivered (under separate cover) to RADC are also identified in Appendix A.

## II. FIRST CONTRACT YEAR

### A. BACKGROUND AND THEORY

The refractive index of a physical system is not independent of the system's absorption coefficient; rather, because of causality, the two are related by an integral transform, known as the Kramers-Kronig relation:<sup>4</sup>

$$n(\omega) = 1 + \frac{c}{\pi} P \int_{-\infty}^{+\infty} \frac{\alpha(\omega') d\omega'}{(\omega')^2 - \omega^2}, \quad (1)$$

where  $\omega$  is the angular frequency of the light,  $n(\omega)$  is the refractive index,  $\lambda$  is the (vacuum) wavelength,  $\alpha(\omega)$  is the absorption coefficient, and  $P$  indicates the principal value integral. In quantum-well systems, where there are nearly discrete absorption features associated with the formation of excitons (bound electron-hole pairs), the implication of Eq. (1) is that there can be a significant contribution to the refractive index due to excitons at a frequency well away from that of the exciton resonance<sup>5</sup>. The excitonic features in quantum wells are known to shift in energy with application of an electric field;<sup>1</sup> this field-induced energy shift is known as the quantum-confined Stark effect (QCSE). Based on the above, the QCSE can be used (in principle) to modulate the refractive index in a wavelength region in which the absorption coefficient of the quantum wells is small.

The ACQW geometry was chosen as a potentially efficient system for electrically modulating the excitonic contribution to the absorption coefficient (and thus the index of refraction). Figure 1a shows an energy-level diagram for the configuration at zero field. If an external field is applied to the left in the figure, the energies of the lowest-energy electron subbands associated with each of the wells approach one another, whereas the lowest-energy hole subband associated with the wide well remains isolated in energy from

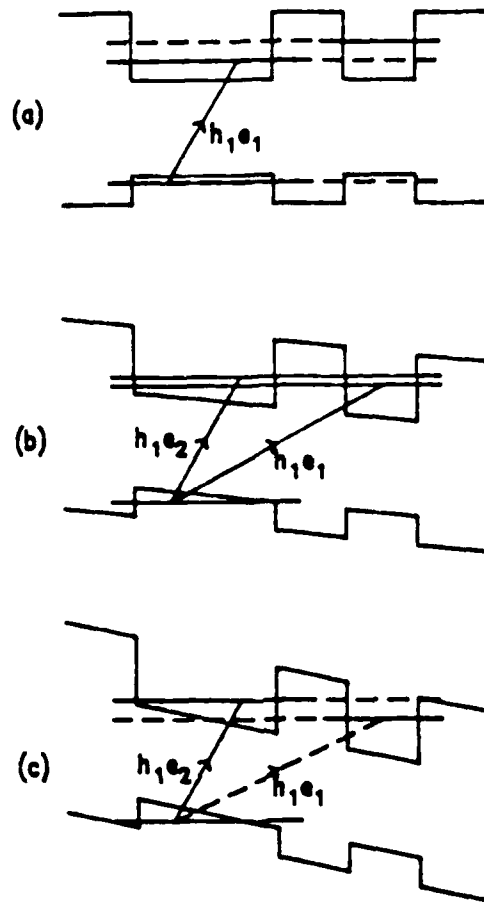


FIG. 1. Schematic diagram of the asymmetric coupled-quantum-well (ACQW) structure, with the applied field equal to (a) zero, (b) the resonance field, and (c) some value beyond resonance. Optical transitions supported by the system are indicated by arrows. Near zero bias, the inter-well transition between the wide-well hole state and the narrow-well electron state is not observed. As the field approaches the resonance field, the energies of the lowest energy electron-states associated with each of the wells approach one another, whereas the lowest energy hole-state remains well separated from other hole states for all field magnitudes. At resonance, there is an avoided crossing of the electron levels and a corresponding delocalization of the electron wave functions; near resonance, both transitions shown are strong. Beyond resonance, the electrons are once again delocalized, but the transition between the hole state of the wide well and the electron state of the narrow well (indicated by the dashed arrow), although weak compared with the intra-well transition, is the lowest energy electron-hole transition supported by the ACQW system.

other hole subbands for all field magnitudes. In Figure 1b, the field magnitude is equal to the resonance field  $F_r$  for which the two electron subbands are in resonance, leading to a minimum splitting of the electron energies and a delocalization of the electron wave functions. Beyond resonance, the electrons are once again delocalized, but the transition (Fig. 1c) between the hole subband of the wide well and the electron subband of the narrow well is now the lowest-energy electron-hole transition supported by the ACQW system and dominates its below-bandgap optical properties.

In our theoretical treatment of this system, we have used the standard envelope-function approximation,<sup>6</sup> (ignoring conduction-band nonparabolicity<sup>7</sup> and valence-band mixing<sup>8</sup>). In our previous report,<sup>3</sup> we described in detail the calculation of electron and hole subband energies and wave functions and of the exciton binding energies and oscillator strengths as functions of applied bias in a GaAs/AlGaAs ACQW structure containing 10- and 5-nm wells and a 2.5-nm barrier.

## B. EXPERIMENT

Experimental results reported for the first year of the contract were obtained primarily through bias-dependent optical absorption (electro-absorption) measurements. Such measurements are an extremely powerful tool for analysis of quantum-well systems because they can provide the energies and strengths of the exciton absorption features, and they reveal the way in which these quantities vary with the applied electric field. This information can be compared directly with theory and can be used to optimize device design parameters.

Typically, the samples used for optical absorption measurements must contain many quantum wells in order to exhibit appreciable optical absorption (on the order of 40 periods of a structure is typical). The samples are fabricated into circular mesa diodes

appropriate for biasing measurements, as described in detail in our previous report.<sup>3</sup> The substrates must be removed to permit transmission of light through the samples. Figure 2 shows a diode processed in this way and illuminated from the back with white light. The diode is highly transmitting in the infrared, but the film used for this picture records only the (relatively weak) portion of the visible spectrum that is not absorbed by the AlGaAs layers.

Among the first samples containing coupled quantum wells that we examined for the contract was one sample containing 8- and 4-nm GaAs quantum wells separated by a 5-nm AlGaAs barrier (sample 259 in Appendix A). This sample exhibited an unusual optical nonlinearity<sup>9</sup> in that the observed Stark shift was much less than that predicted theoretically and depended strongly on the intensity of the light used to probe the sample.

We provided a tentative (and somewhat incomplete) explanation of this effect<sup>9</sup> in terms of a charge separation and a resulting cancellation of the applied fields that occurs when the coupled-well system is biased beyond resonance. Although the origin of this nonlinearity is still not fully understood, we now believe that it arose from the relatively poor quality of sample 259 and other samples grown in our molecular-beam epitaxy (MBE) system around the same time and is not a fundamental property of the ACQW system. These samples had a relatively high Al mole fraction in the AlGaAs layers and exhibited a high density of deep levels that could act as long-lived carrier traps. The presence of such traps may explain the long recombination times needed to fully quantify the nonlinearities.

For similar reasons, we now believe that the complete suppression of any Stark shifts described in our previous report<sup>3</sup> for a GaAs/AlGaAs ACQW structure with a 0.8-nm barrier (sample 351) is a result of a high density of deep levels in the AlGaAs. We have since grown several ACQW samples with thin barriers that show large Stark shifts.



FIG. 2. Micrograph of a 250- $\mu$ m-diameter mesa diode processed for transmission measurements by removing the GaAs substrate. The diode was illuminated from the back with white light, and the film recorded only the portion of the visible spectrum that was not absorbed by the AlGaAs layers in the sample. (The film was not sensitive to the strong infrared light transmitted by the diode.)



Samples grown much later on the MBE had much lower deep level densities; correspondingly, later quantum-well samples did not exhibit any such nonlinear effects, and therefore the effects did not interfere with the observation of the coupling mechanisms that are of interest for this contract.

### III. RESULTS FOR GaAs/AlGaAs STRUCTURES

#### A. IMPLICATIONS OF LOW-TEMPERATURE PHOTOCURRENT MEASUREMENTS

The experimental results obtained during the first contract year were not altogether encouraging, for several reasons. First, samples grown early in the contract period tended to exhibit unusual effects that masked the features of interest (see the prior discussion of nonlinear effects). Second, the use of transmission measurements as the primary tool for studying the electro-absorption properties of ACQWs introduced unnecessary (as it turned out) complexities into the processing of samples for experiments. As a result of these (and other) problems, we were unable, during the first year of the contract, to observe unambiguous evidence of the well-coupling phenomena that we sought to establish.

In an attempt to circumvent some of these difficulties, we explored (partially under internal funding and partially under funding from this contract) the use of room- and low-temperature photocurrent (PC) measurements<sup>10</sup> as an alternative to transmission measurements. The observed PC in a p-i-n diode structure is given by<sup>11</sup>

$$I(\lambda) = \frac{e\lambda W(\lambda)}{hc} (1 - r) \left\{ 1 - \exp[-\alpha(\lambda)L] \right\} \eta(\lambda) , \quad (2)$$

where  $I(\lambda)$  is the collected photocurrent,  $W(\lambda)$  is the power of the incident (dispersed) light,  $r$  is the reflectivity of the sample-air interface,  $\alpha(\lambda)$  is the absorption coefficient of the intrinsic region of the diode,  $L$  is the intrinsic region thickness, and  $\eta(\lambda)$  is the carrier collection efficiency of the diode. As long as  $\eta(\lambda)$  is not a strong function of the light wavelength  $\lambda$ , PC is proportional to the absorption spectrum of the diode's intrinsic region.

Using the PC technique greatly simplifies sample processing. There is no need to remove the substrate (since the light does not need to be transmitted through the sample), and diodes are formed simply by depositing a blanket n-type (Au/Sn/Au) contact on the back surface of the wafer and etching mesas (on the order of 5  $\mu\text{m}$  in height) with p-type (Au/Cr/Au) ring contacts. Typically many diodes are processed on a single piece of material, and current-voltage characteristics are measured at room temperature to identify diodes with good electrical properties (high reverse-bias breakdown voltages, low leakage currents, etc.).

An initial PC study<sup>12</sup> pointed out potential difficulties associated with background doping in p-i-n diode samples with relatively thick intrinsic regions. Such difficulties had been suggested by theoretical calculations,<sup>13</sup> but no previous quantitative comparison with experiment had been made prior to our study. The PC experiments were performed on two samples, one an ACQW structure with thick barriers and the other containing many wells of a single width. This work was not supported by the contract, but the results are relevant to the contract work and are reported here.

The layer sequence for the samples, starting from the substrate, is as follows: 0.5- $\mu\text{m}$   $n^+$  GaAs buffer, 1.0- $\mu\text{m}$   $n^+$  AlGaAs etch stop (to allow substrate removal for transmission studies), 0.22  $\mu\text{m}$  each of n-doped and undoped superlattice serving as a barrier for dopant migration during growth, the MQW structure itself, another 0.09  $\mu\text{m}$  each of undoped and p-doped superlattice, and a thin  $p^+$  GaAs contact layer. For the ACQW sample (sample 802 in Appendix A), the quantum-well region consists of 40 periods of a 3.6-nm GaAs well, a 9.0-nm AlGaAs barrier, an 8.8-nm GaAs well, and a 9.8-nm AlGaAs barrier. The total thickness of the intrinsic region, including undoped superlattice, is 1.55  $\mu\text{m}$ . This sample was originally grown as a control for studying the properties of the wide and narrow wells in the absence of coupling. Sample 800 has 40 GaAs wells, each 7.2-nm

thick, separated by 9.8-nm barriers, and a total intrinsic-region thickness of 0.98  $\mu\text{m}$ . In both cases the Al mole fraction in the AlGaAs is 0.26. The well widths were determined by comparing the peak energies of the heavy-hole exciton features observed in the zero-field low-temperature PC spectra with single-band envelope-function calculations.

After growth, the samples were processed into 250- $\mu\text{m}$ -diameter mesa diodes with p-type ohmic contact rings (100- $\mu\text{m}$  inner diameter) on the top surface. Room-temperature capacitance-voltage measurements on sample 802 gave a background carrier density of  $4.5 \times 10^{15}/\text{cm}^3$ ; the bias necessary to fully deplete its intrinsic region is about 6 V at room temperature.

Both samples were characterized using low-temperature, field-dependent PC and photoluminescence (PL) spectroscopy. Figure 3 shows the 8-K PL spectra from sample 802 at reverse biases of 0, 2, 8, 12, and 14 V. At low bias voltages, a strong peak ( $h_1e_1$ ) and a weak peak ( $l_1e_1$ ) associated with the 8.8-nm well are observed. Figure 4 shows the low-temperature PC spectra (at the same biases) for the same sample. The zero-bias curve in Fig. 4 shows strong absorptions at nearly the same energies as those in Fig. 3. As the reverse bias increases, the peaks in the PC spectra broaden considerably, and a set of subsidiary peaks forms at lower energies. At a 14-V reverse bias, there are four distinct peaks in the PC spectrum between 1.52 and 1.56 eV; the corresponding PL spectrum has only one peak. In addition, the PC spectrum shows Stark shifts of the heavy-hole exciton of up to 50 meV at 20 V reverse bias, whereas the PL spectrum shows only a 15-meV shift.

The difference between the observed bias dependence of the PL and PC spectra can be explained in terms of the depletion characteristics of the quantum-well region arising from unintentional background doping. The PL is due predominantly to carrier recombination in the undepleted (zero-field) region near the surface of the sample. In the

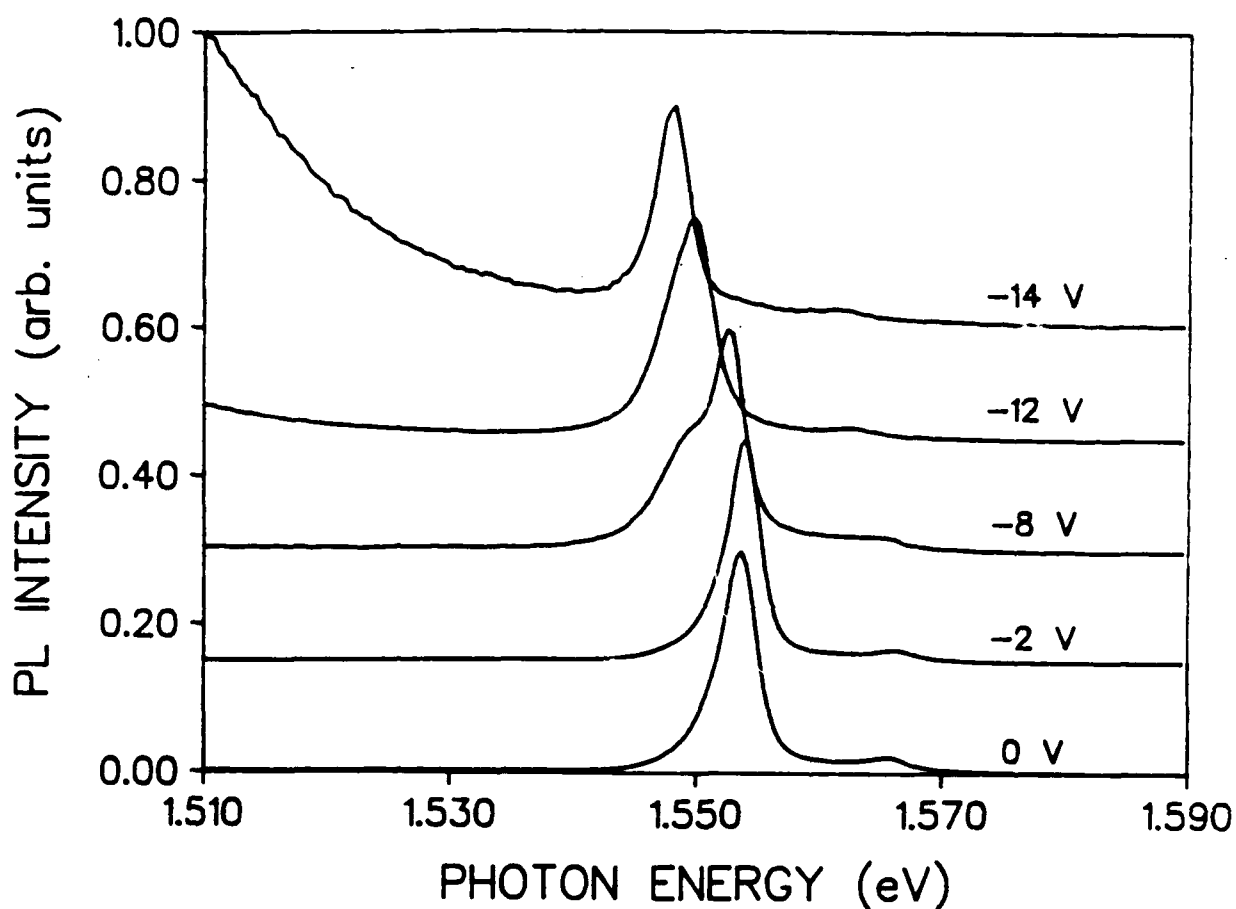


FIG. 3. Bias-dependent, 8-K photoluminescence (PL) spectra from a p-i-n diode (sample 802) containing the ACQW structure with 8.8-nm-thick wide wells and thick (9.0-nm) barriers; the total intrinsic-region thickness is 1.55  $\mu\text{m}$ . Curves have been individually normalized and offset for clarity. (The peak PL intensities actually span two orders of magnitude for the bias range shown.)

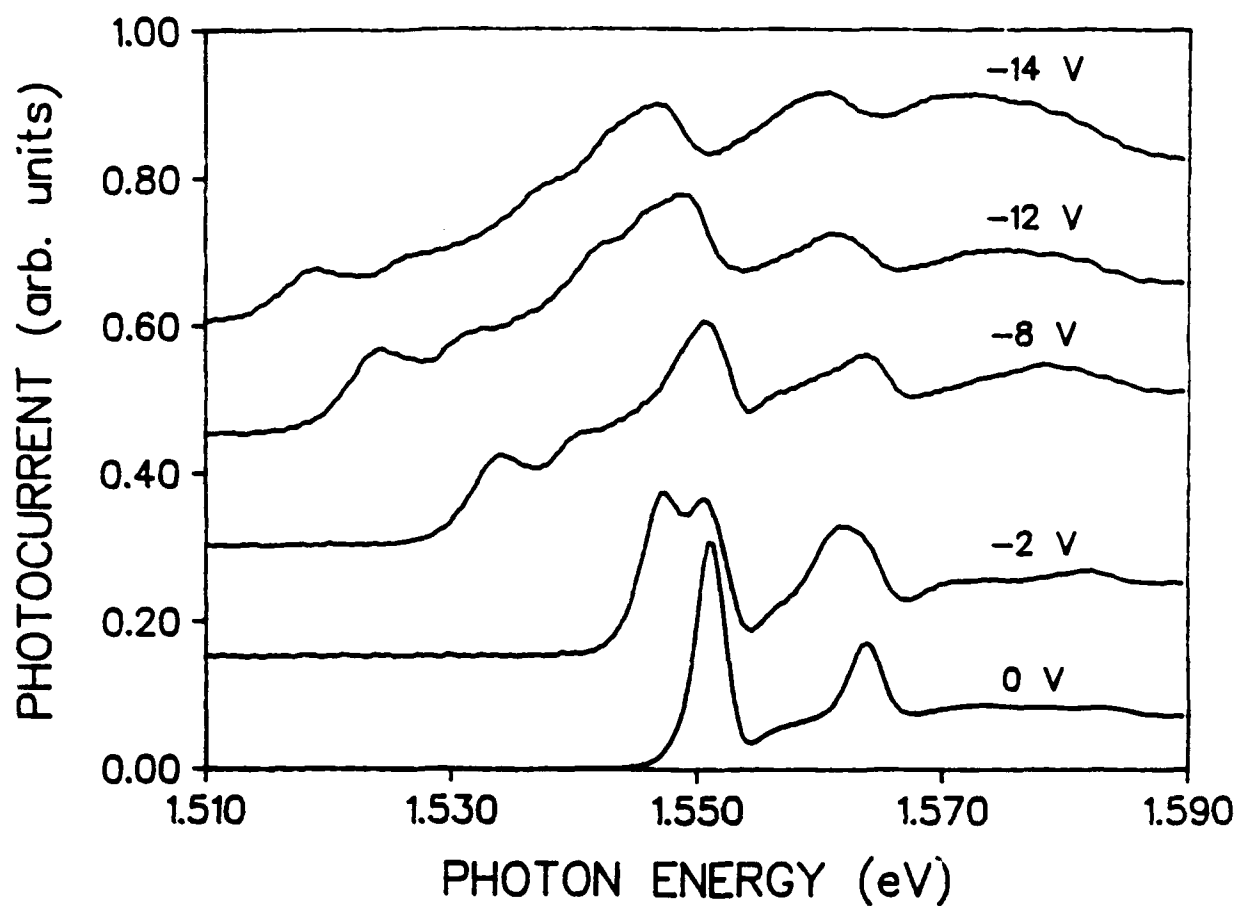


FIG. 4. Bias-dependent, 8-K photocurrent spectra from sample 802. The presence of several peaks at large reverse biases where there is only one in the PL spectrum indicates the presence of a substantial electric-field inhomogeneity.

depleted region, photogenerated carriers are swept away by the internal field, so that the recombination efficiency is lower than that of the field-free region. However, the PC is most efficiently generated in the high-field regions of the sample, wherein the electrons and holes can be efficiently swept toward the contact layers by the electric field and collected. Low-field features can also be observed in PC spectra because some of the charges generated in the undepleted quantum wells diffuse into the high-field region, where they can be collected.

The electric-field distribution within the MQW region was calculated by assuming that the background doping in the intrinsic region is slightly p-type (arising from the incorporation of carbon into the structure during growth) and by using a standard depletion model<sup>14</sup> for a  $p^-/n^+$  junction. The Stark shifts in the quantum-well transitions were calculated as functions of the electric field by using the single-band envelope-function approximation, with the background doping density and the intrinsic-region thickness taken as adjustable parameters. Because field-dependent changes in the exciton binding energies are generally small compared with Stark shifts of the electron and hole subbands, they have been neglected.

According to the model, for biases below that necessary to fully deplete the intrinsic region of the diode, the minimum field in the MQW region (experienced by the quantum wells within the undepleted region) is zero, and there should be a corresponding unshifted exciton peak. This is confirmed by both the PL and PC spectra (see Figs. 3 and 4 for biases up to 8 V). If we assume that the lowest- and highest-energy heavy-hole peaks in the PC spectra correspond to the minimum and maximum fields in the MQW region, a quantitative comparison of theory and experiment is possible. This is shown in Fig. 5, where we compare calculations of the minimum and maximum  $h_1e_1$  transition energies as functions of applied bias with experimental peak positions taken from the PC spectra for

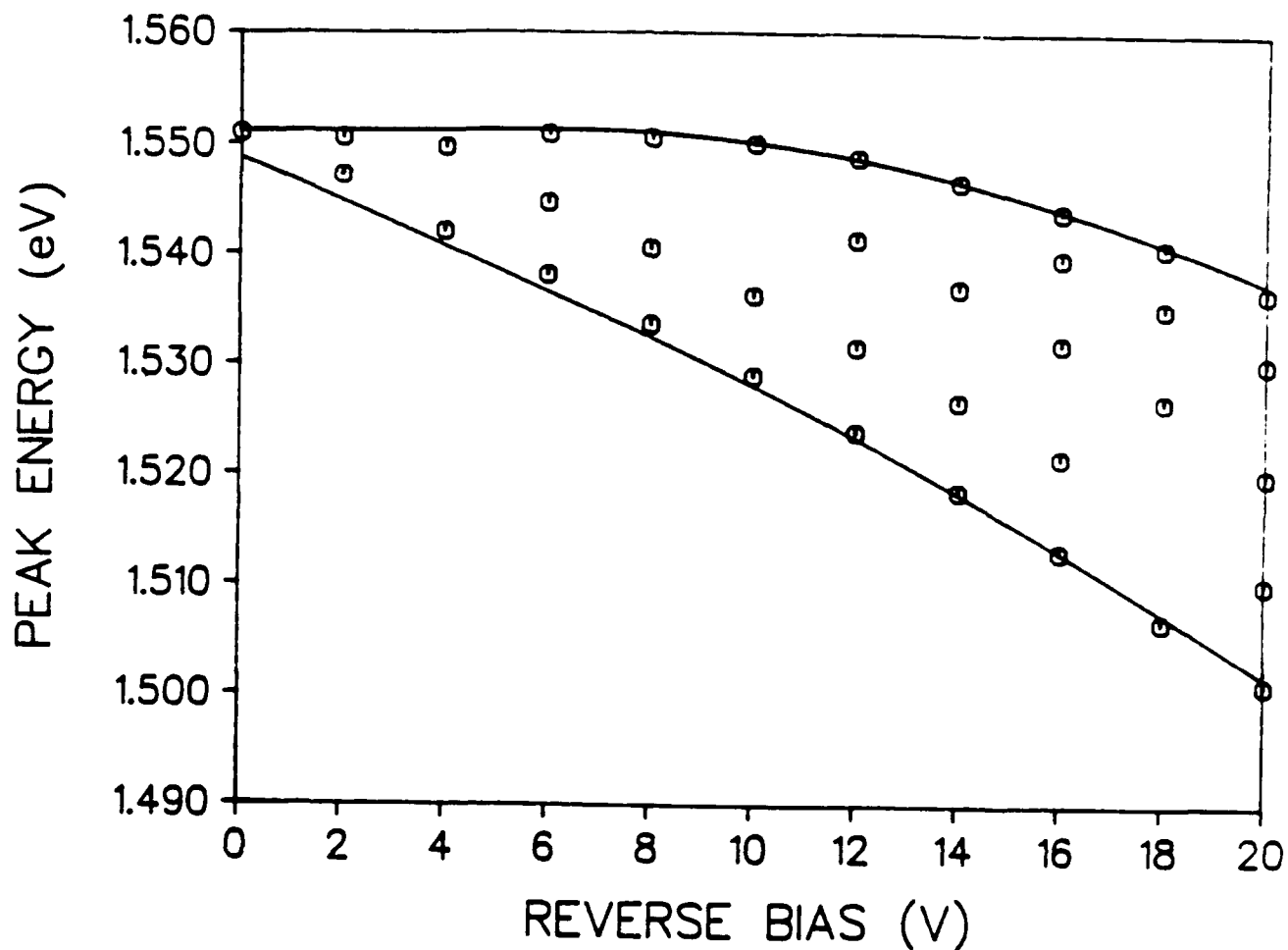


FIG. 5. Measured (symbols) and calculated (solid lines) energies of the  $h_1e_1$  transition as a function of applied bias for sample 802. The calculated energies are for the quantum wells that experience the minimum and maximum electric fields; experimental points (from the photocurrent spectra) are plotted for all distinguishable peaks.



sample 802, with the background doping  $p = 5.63 \times 10^{15}/\text{cm}^3$  and intrinsic-region thickness  $d = 1.542 \mu\text{m}$ . Figure 6 shows a similar comparison for sample 800, which had a thinner intrinsic region and narrower wells, where we have taken  $p = 4.74 \times 10^{15}/\text{cm}^3$  and  $d = 0.914 \mu\text{m}$ . As seen in Fig. 5 (and in Fig. 4 as well), the "spreading" observed in sample 802 (the thicker sample) consists in fact of a series of a few peaks. This series may arise from a "locking" effect in which many wells cluster into domains, all of which see the same field. Such an effect may be necessary in order to satisfy the condition of conservation of tunneling current between wells;<sup>15</sup> in any event, it is beyond the scope of the present work.

For reverse biases greater than that necessary to deplete the intrinsic region, the difference in electric fields between the lowest-field and the highest-field regions is about 100 kV/cm in sample 802 and 50 kV/cm in sample 800. The spread in peak energies observed for sample 800 was much less than for sample 802 because the narrower wells experienced smaller Stark shifts and the range of fields within its MQW region was smaller. The agreement of the calculations with the experimental data is excellent, and the adjustable parameters are all within 10 % of their design values (which is fully satisfactory given the crudeness of the model).

The background doping observed in these samples is somewhat high, although in the typical MBE growth range.<sup>16</sup> It is an unavoidable consequence of background impurities present in the growth chamber that are incorporated into the device structure during growth. Since the PC technique is sufficiently sensitive to characterize structures containing only a few wells, the "smearing" effects associated with the background can be minimized by growing samples that contain 5-10 wells and that therefore have a much lower field inhomogeneity in the MQW region. Since the quantum-well waveguides that are of interest for phase-shifting devices meet these requirements, all the GaAs/AlGaAs samples

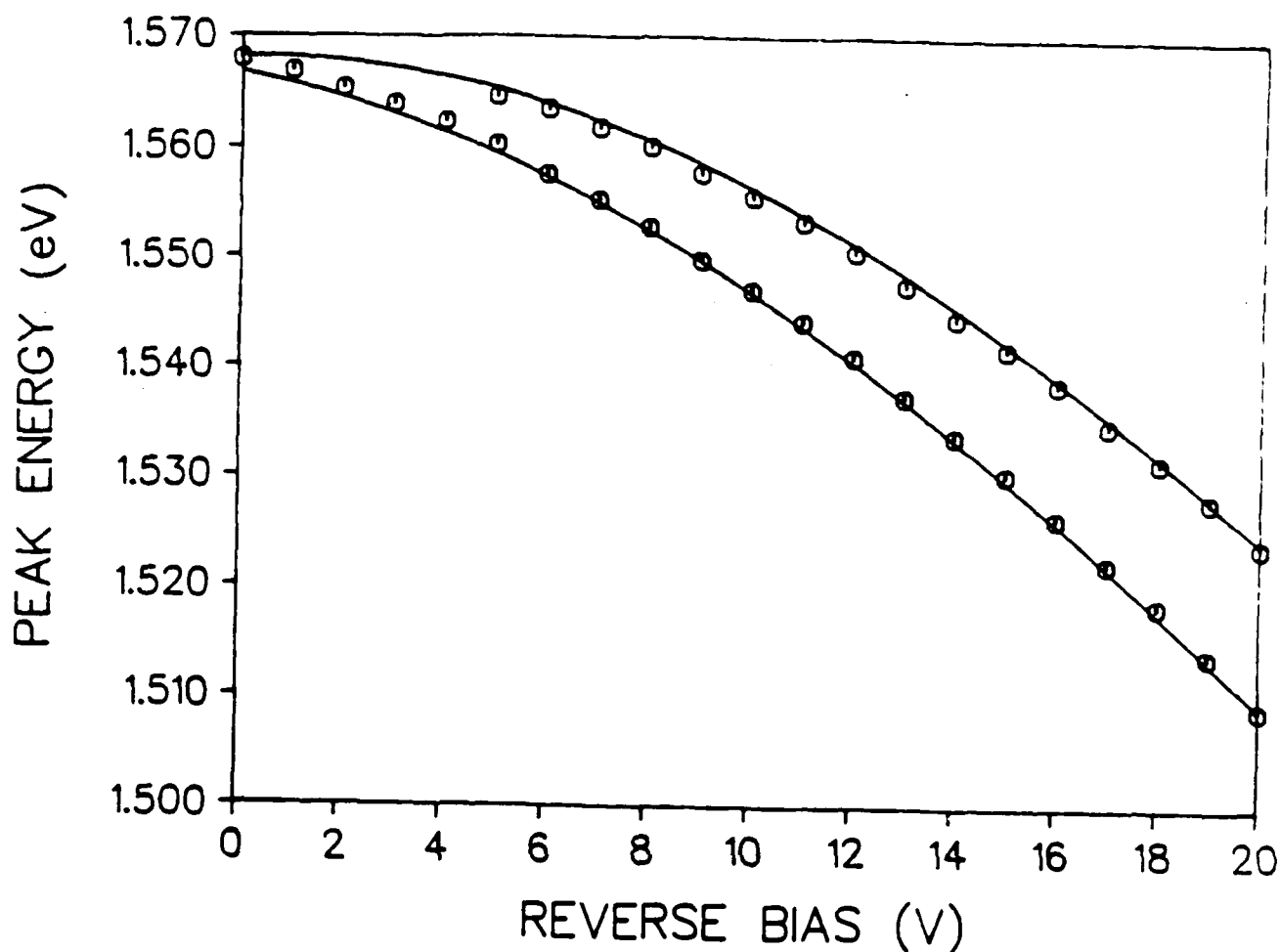


FIG. 6. Measured (symbols) and calculated (solid lines) energies of the  $h_1e_1$  transition as a function of applied bias for a p-i-n diode (sample 800) containing 40 GaAs wells, each with a thickness of 7.2 nm, separated by 9.8-nm barriers. Because the intrinsic region of this sample (0.98  $\mu\text{m}$ ) is much smaller than that of sample 802, the corresponding electric-field inhomogeneity is much smaller.

grown for the contract after our initial PC studies were of this form and were useful both for fundamental studies of the electronic states in the quantum wells and for fabrication of waveguides for phase-shift and absorption modulation measurements.

## B. OBSERVATION OF COUPLING EFFECTS IN GaAs/AlGaAs ACQW STRUCTURES

Since the beginning of the contract period, there have been several publications by others on the optical properties of coupled quantum-well structures,<sup>17-22</sup> although most of this work has been concerned with symmetric or slightly asymmetric systems. Low-temperature, high-resolution spectroscopic studies of symmetric<sup>21</sup> and slightly asymmetric<sup>22</sup> systems demonstrated an abundance of spectral features resulting from the breakdown of selection rules appropriate for isolated quantum wells. This spectral richness has tended to hinder the unambiguous interpretation of the observed phenomena and has therefore prevented detailed comparisons of theory with experiment in these systems.

Having overcome the problems discussed in Section III.A, which inhibited our studies of coupling effects in the ACQW system, we were able to grow samples in which the effects of electron coupling between wells was demonstrated unambiguously in low-temperature PC measurements.<sup>23</sup> In contrast to the studies referred to in the above paragraph, in our work the ACQW system has a relatively large degree of asymmetry. As we report here, the field dependence of optical transitions in this system displays the effects of the coupling between electron levels without the simultaneous hole coupling that occurs in nearly symmetric coupled-well systems.<sup>19-22</sup> As a result, a detailed comparison of calculations with experiment is possible, enabling, e.g., a determination of the band offsets in the GaAs-AlGaAs system.

The quantum-well region of the sample used in this study (1121 in Appendix A) consists of seven periods of the ACQW structure (9.5-nm GaAs well, 2.4-nm AlGaAs barrier, 4.5-nm GaAs well, and a 9.8-nm AlGaAs spacer layer). This undoped structure is imbedded in a p-i-n diode for reverse biasing. We determined the thicknesses and compositions of the well and barrier layers by measuring the energies of the AlGaAs absorption edge (to determine the Al mole fraction) and the lowest-energy excitonic transition in the wide well (to determine its width) using PC spectroscopy under a slight forward bias (i.e., nearly flat-band). These two parameters gave the absolute growth rates for GaAs and AlGaAs, which we used along with programmed shutter times to determine all other layer thicknesses. These thicknesses and compositions are consistent with growth rates and Al mole fractions determined from calibration samples and with transmission electron microscopy measurements (of layer thicknesses) of the sample (see Fig. 7).

The sample was processed into mesa diodes as described in Section III.A. Figure 8 shows the 8-K PC spectra in the 1.52-1.57-eV region for three applied biases corresponding to fields below, at, and above the resonance of the electron subbands in the two wells. (The curves have been offset vertically for clarity.) All the features observed in this spectral region arise from transitions involving hole subbands localized in the wide well. Features above 1.6 eV (not shown here) include narrow-well and excited-state wide-well transitions and show the effects of coupling between both electron and (excited-state) hole levels. Optical nonlinearities, discussed in Section II, were not observed in the present sample for the light intensities used in these experiments.

At zero bias, the transitions labeled  $h_1e_1$  and  $l_1e_1$  are quite sharp, with a full width at half-maximum of  $\sim 2.1$  meV. At a reverse bias of 3.22 V, the coupling of the electron levels in the two wells results in significant oscillator strength in all transitions between the localized hole subbands ( $h_1$ ,  $l_1$ , and  $h_2$ ) and the pair of delocalized electron subbands.



FIG. 7. Transmission electron micrograph of the ACQW region of sample 1121. The light layers are AlGaAs, and the dark layers are the GaAs quantum wells.

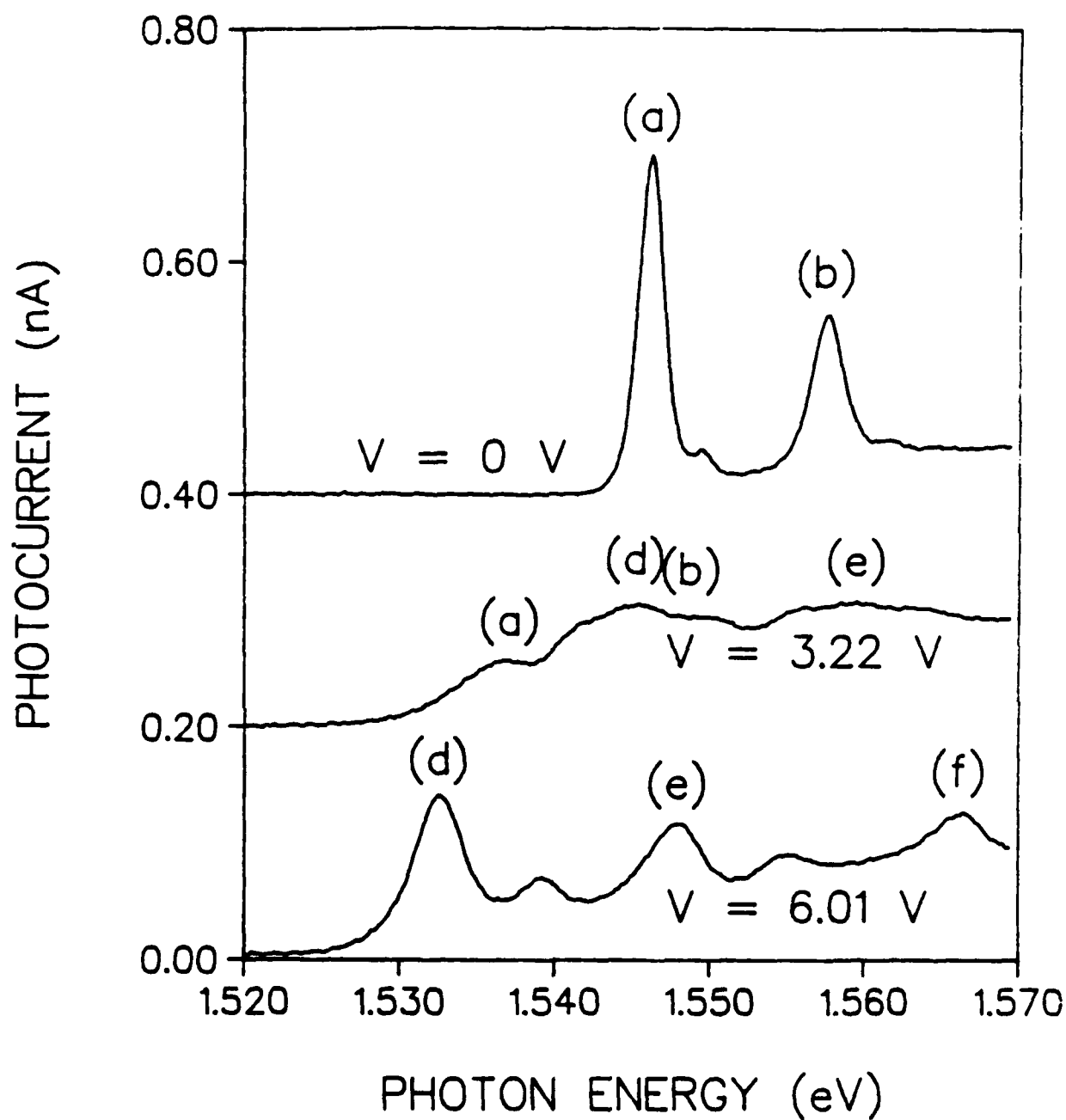


FIG. 8. 8-K photocurrent spectra of the GaAs/AlGaAs ACQW sample (sample 1121) at three values of the applied reverse bias: 0 V, 3.22 V, and 6.01 V. Transitions of interest are labelled as follows: (a)  $h_1e_1$ ; (b)  $l_1e_1$ ; (c)  $h_2e_1$ ; (d)  $h_1e_2$ ; (e)  $l_1e_2$ ; and (f)  $h_2e_2$ .

The transitions  $h_2e_1$  and  $h_2e_2$  correspond to isolated-well transitions that are forbidden by symmetry for zero field, but are allowed for non-zero fields.<sup>10</sup> The dominant features in the spectrum for 6.01-V reverse bias are the  $h_1e_2$ ,  $l_1e_2$ , and  $h_2e_2$  transitions (see Fig. 1). The small peaks on the high-energy side of each of the main features arise from the last wide well of the seven coupled-well pairs, which was  $\sim 0.5$  nm narrower than the others due to an error in shutter timing during growth.

Figure 9 shows the peak energies of the transitions of interest as a function of applied reverse bias. The avoided level crossing associated with the interaction of electron subbands is seen in the  $h_1$  and  $l_1$  transitions for reverse biases between 2 and 4 V. Also shown in Fig. 9 are the calculated peak energies determined by a single-band envelope-function approximation, with the assumption that 70% of the GaAs-AlGaAs energy-gap discontinuity occurs in the conduction band. Field-independent exciton binding energies of 8 and 12 meV were used, respectively, for heavy- and light-hole transitions. A linear relationship was assumed between internal electric field (the theoretical parameter) and applied bias (the experimental parameter). We determined a built-in diode potential of 1.9 V from the 77-K current-voltage characteristics of the diodes, and an effective intrinsic-region thickness of 0.92  $\mu\text{m}$  by matching the calculated and measured quantum Stark shifts of the "allowed" heavy-hole transition in the high-field region, well away from resonance. This latter value is consistent with results of room-temperature capacitance-voltage measurements performed on the sample.

Figure 9 shows that the observed phenomena are associated with the avoided level crossing of the electron subbands. The experimental values of the minimum energy splitting of electron levels and the bias voltage at which the minimum occurs are  $9.4 \pm 0.3$  meV and  $3.24 \pm 0.10$  V, respectively. (These were obtained by fitting the average of the splittings obtained from the "allowed" light- and heavy-hole transitions in the vicinity of

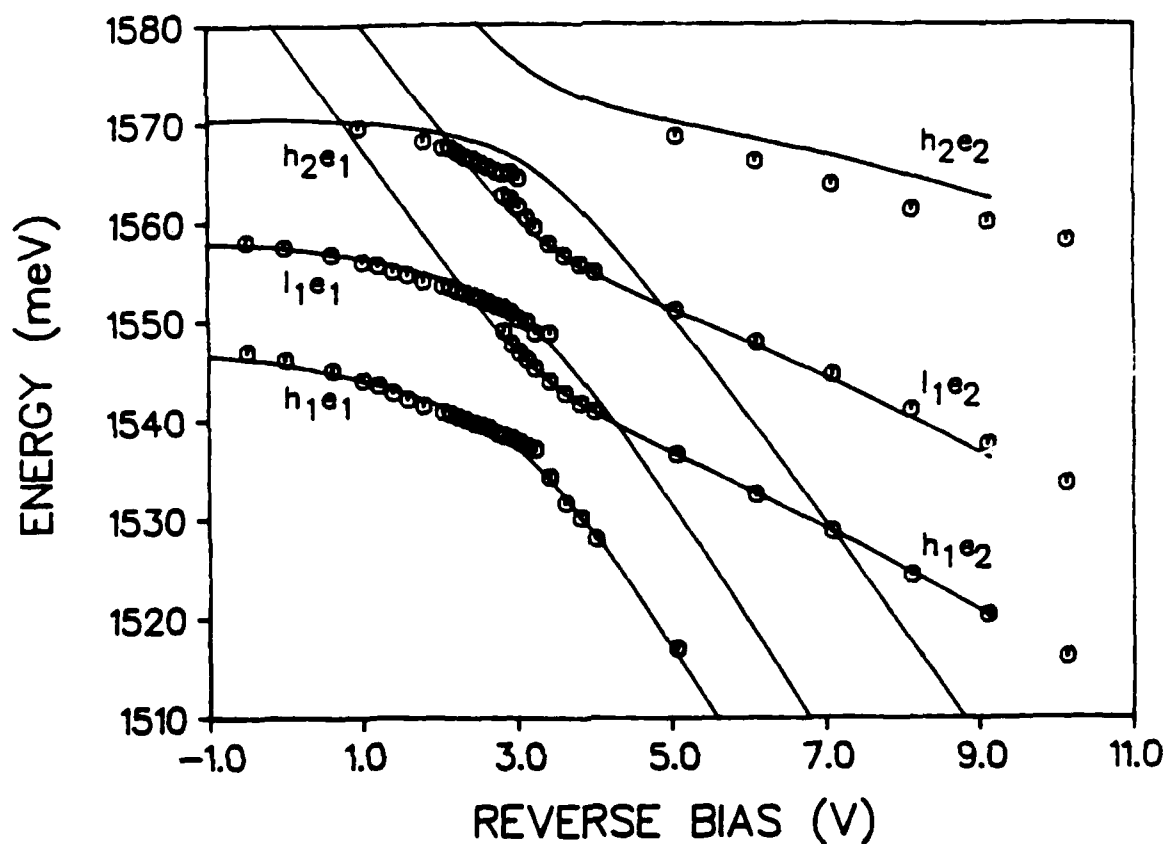


FIG. 9. Observed (symbols) and calculated (solid lines) peak transition energies as functions of applied reverse bias in sample 1121. In the calculations, the applied bias was determined from the electric field by using the expression  $V = -1.9 + 0.092E$ , where  $V$  is in V and  $E$  is in kV/cm (see text).



the crossing, as a function of bias voltage, to a parabolic form.) The calculated splitting, 9.7 meV, and crossing bias, 3.25 V, are in excellent agreement with the experimental results. Generally, for the forbidden transitions ( $\hbar_2 e_{1,2}$ ), the difference between calculated and observed transitions is on the order of 2-3 meV. The agreement is much better than this for the "allowed" transitions, even in the resonance region.

The calculated values for the minimum electron energy splitting and the crossing bias are strong functions of the height of the conduction-band barrier. By repeating the energy-level calculations for a number of different values of the barrier height we were able to deduce that a conduction-band offset of 70% of the energy-gap discontinuity was consistent with the experimental data. (For comparison, the calculated minimum splittings and crossing voltages are 12.4 meV and 2.13 V, respectively, for a 50% offset and 8.6 meV and 3.98 V, respectively, for an 80% offset.) Previous results for the band offset varied from 85%<sup>24</sup> to 55%,<sup>25</sup> and the most recently reported results are in the 60-65% range.<sup>26,27</sup> In our past calculations, we consistently used the 70% figure, and the present results increase our confidence in this value.

The highly asymmetric system investigated under the present contract has many advantages over symmetric (or slightly asymmetric) systems for studying the details of coupling between quantum wells. As shown in Fig. 1, it is possible to electrically tune the system completely through the resonance, which is not possible with nearly symmetric systems, where the simultaneous coupling of hole and electron subbands greatly complicates the interpretation of the absorption spectra.<sup>21,22</sup> As seen in Fig. 9, the use of an ACQW system with a low density of deep levels and a relatively thin MQW region has enabled us to overcome the difficulties encountered in previous samples and unambiguously interpret the optical transitions as a function of applied bias. In addition, the excellent agreement between the experimental results and the theoretical calculations provides

credence to our interpretation of results on waveguide phase shifts in similar samples and has allowed us to design structures in the InGaAs/InAlAs materials system that exhibit similar effects.

### C. ELECTRO-ABSORPTION AND ELECTRO-REFRACTION IN GaAs/AlGaAs ACQW WAVEGUIDES

The ACQW system has been shown (see Section III.B above) to exhibit novel electro-optic properties associated with the coupling of subbands in the two wells. Here, we show that the inter-well transition, beyond the resonance field, dramatically affects the electro-absorption and electro-refraction properties of waveguides made from ACQW structures.

There have been several studies of the phase-shifting properties of GaAs/AlGaAs waveguides containing quantum wells. Glick *et al.* reported the electro-optic properties of a multi-mode waveguide containing 30 GaAs wells, each 12.2-nm thick, at wavelengths of 1.1523 and 0.888  $\mu\text{m}$ .<sup>28,29</sup> At the longer wavelength, the observed electro-optic effect was linear with applied bias; this wavelength is too far removed from the sample's absorption edge for the quantum wells to have any effect, and the observed electro-optic coefficient was close to that of bulk GaAs.<sup>28</sup> At 0.888  $\mu\text{m}$ , a large quadratic electro-optic coefficient was measured, which was attributed to the QCSE. Single-mode leaky guides containing a pair of 9.4-nm quantum wells showed similar results at 0.850  $\mu\text{m}$ .<sup>30</sup> Later, Zucker *et al.*<sup>31</sup> studied the same sample at wavelengths between 0.82 and 0.88  $\mu\text{m}$  using a Mach-Zehnder interferometer. They reported a large dispersion in both the linear and quadratic electro-optic coefficients and observed a strong spectral dependence in the so-called "chirp parameter," given by  $\Delta n/\Delta k$ , where  $n$  and  $k$  are the real and imaginary parts of the index of refraction.

Here we consider a similar study of the electro-absorption and electro-refraction properties of single-mode waveguides containing the ACQW structure. Figure 10 shows the energies of the optical transitions from the wide-well light-hole subbands to the pair of coupled electron subbands as a function of applied bias in this structure. The lines are dashed in regions where the corresponding transitions are weak, and are solid otherwise. Well beyond resonance, the solid line represents the transition to the electron subband that is localized mainly in the wide well. Its transition energy decreases quadratically with increasing bias due to the QCSE. The dashed line in this region represents the transition to the electron subband localized (predominantly) in the narrow well. The dependence of the energy of this inter-well transition on applied bias is approximately linear because of the spatial separation of the hole and electron subband envelope functions, which introduces a dipole-type term into the expression for the transition energy.

The quantum-well waveguide sample used<sup>32</sup> for this study (sample 919 in Appendix A) consisted of seven periods of the ACQW structure imbedded in a p-i-n diode. The thicknesses of the layers that constitute one period are as follows: 8.5-nm GaAs wide well, 2.1-nm AlGaAs barrier, 4.3-nm GaAs narrow well, and an 8.5-nm-wide AlGaAs barrier between the pairs of coupled wells. The cladding regions consisted of 1.5- $\mu\text{m}$   $\text{Al}_{0.32}\text{Ga}_{0.68}\text{As}$  layers, doped n+ and p+ (below and above, respectively) to 0.65  $\mu\text{m}$  from the guiding (multi-quantum well) region. This resulted in a single-mode (planar) p-i-n diode waveguide with a 0.19- $\mu\text{m}$ -thick core in the center of a 1.5- $\mu\text{m}$ -thick intrinsic region. The calculated fill factor<sup>3</sup>  $\Gamma$  for this system is 0.148, or 0.0212 per well pair.

To make the sample, the substrate was first thinned to approximately 100  $\mu\text{m}$ , and n- and p-type ohmic contacts (Au/Sn/Au and Au/Cr/Au) were deposited onto the bottom and top surfaces, respectively. (The former was annealed at 310  $^{\circ}\text{C}$  for 30 s, and the latter was not annealed.) Then the material was cleaved into 600- $\mu\text{m}$ -wide bars, and

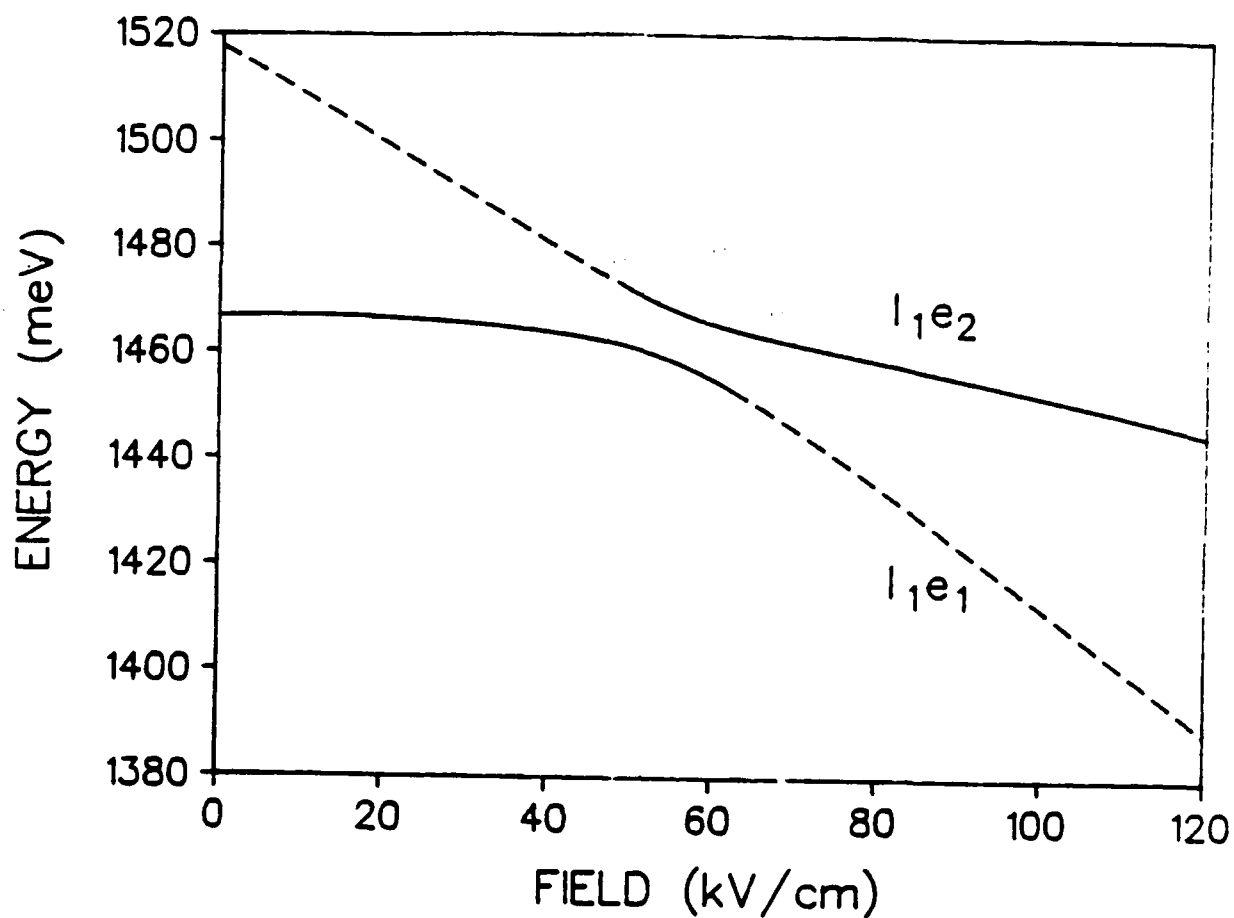


FIG. 10. Calculated energies of the  $l_1e_1$  and  $l_1e_2$  transitions in an ACQW structure (sample 919) with 8.5-nm and 4.3-nm GaAs wells coupled by a 2.1-nm AlGaAs barrier, as functions of the applied electric field. Dashed lines indicate weak absorptions associated with interwell transitions.

individual diodes were formed by dicing with a saw. The diodes were approximately 150- $\mu\text{m}$  wide (and can be considered slab guides for the purpose of this experiment). The reverse-bias breakdown voltage for the diodes used was typically 25 V.

The measurement system consists of a Mach-Zehnder interferometer with a pair of microscope objectives in one arm to end-fire-couple the light from an  $\text{Ar}^+$ -laser-pumped Styryl-9M dye laser into the cleaved facet of a planar ACQW waveguide and to collimate the emerging radiation. The resulting interference pattern was detected by a 0.3-mm-diameter Ge photodiode. The bias was applied to the sample as a 500-Hz square-pulse train with a 50% duty cycle, and a boxcar averager was used to separate the "bias-on" signal from the "bias-off" signal. A PZT piezoelectric transducer was used to move a mirror in the reference arm, allowing us to simultaneously trace several periods of the two interferograms (with and without bias applied to the sample).

Figure 11 shows a typical scan, with the upper curve generated with no voltage on the sample, and the lower curve generated with -4 V on the sample. Each of the interferograms was analyzed assuming

$$I_j = A_j + B_j \sin[f(V_r) + \phi_j] \quad , \quad (3)$$

where  $j = 1$  and 2 correspond to the bias-on and bias-off interferograms, respectively,  $I_j$  is the measured light intensity,  $A_j$  and  $B_j$  are constants,  $f(V_r)$  represents the phase change in the reference arm as a function of the voltage  $V_r$  applied to the PZT, and  $\phi_j$  are the phases with voltage on ( $j = 1$ ) and with voltage off ( $j = 2$ ). In practice, we used a fourth-degree polynomial for  $f(V_r)$  and fit each pair of interferograms using the six constants in Eq. (3) (for  $j = 1$  and 2) together with the polynomial coefficients as fitting parameters. In this way we determined both the phase shift ( $\phi_1 - \phi_2$ ) and the change in transmission  $(B_1/B_2)^2$  as functions of the bias on the sample, with the former being determined to an accuracy of better than 0.5 degrees.

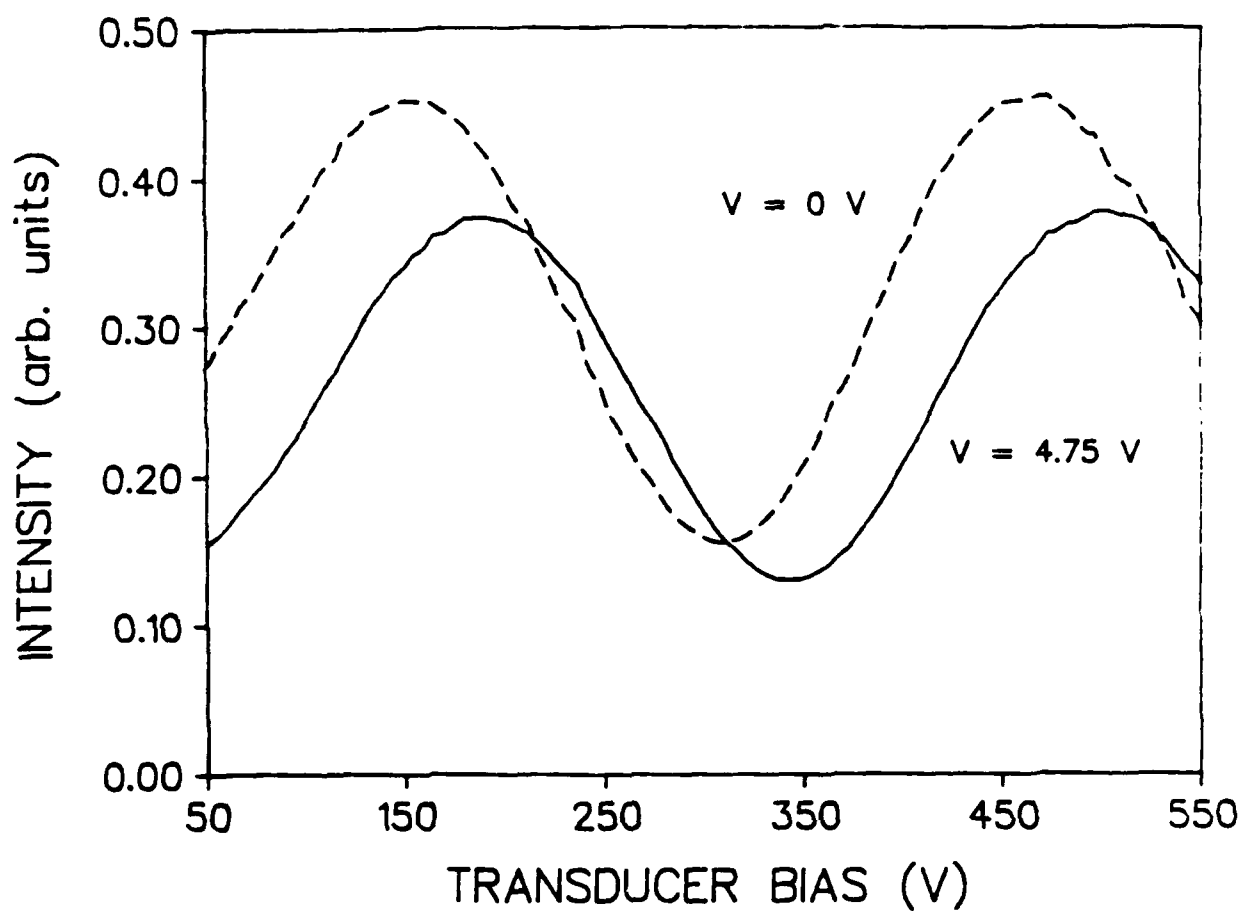
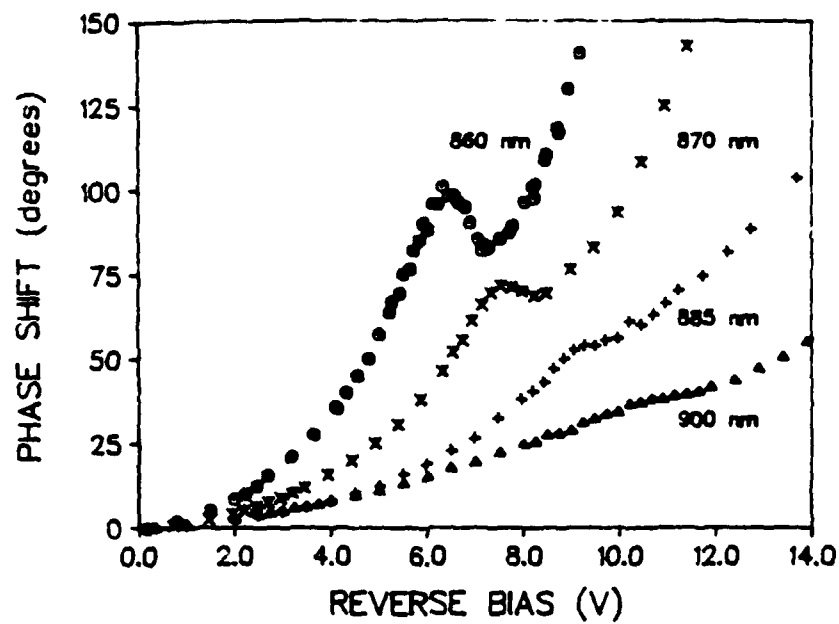


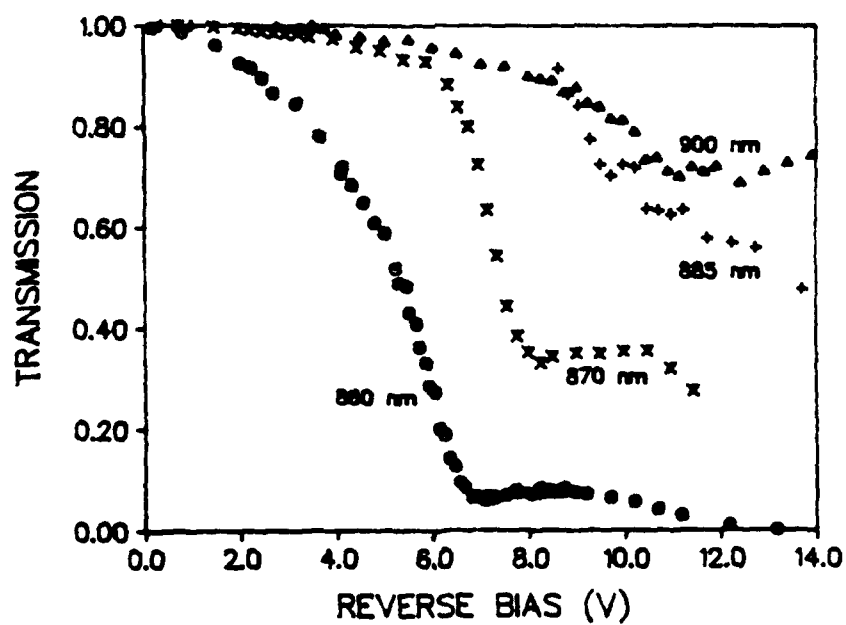
FIG. 11. Interferograms measured in the Mach-Zehnder interferometer with 860-nm-wavelength light. The two scans are displaced due to a phase shift obtained when 4 V reverse bias is applied to an ACQW waveguide fabricated from sample 919.

The results reported here were obtained with the electric vector of the incident light polarized perpendicular to the sample layer interfaces (i.e., TM-polarized). With this polarization, only light-hole-to-electron transitions affect the optical properties of the guide,<sup>5</sup> thus simplifying the interpretation of the observed phenomena. In Fig. 12 we show the results of electro-refraction and electro-absorption measurements made at four laser wavelengths, corresponding to energies of 45, 60, 84, and 107 meV, respectively, below the zero-bias energy of the  $l_1e_1$  exciton, which occurs at a wavelength of about 835 nm. In the phase shift data (a), a distinct feature is apparent (superimposed on a monotonically increasing background) in each of the curves in Fig. 12, which moves to higher biases and becomes weaker as the wavelength increases. The approximately quadratic shape of the background is expected<sup>29-31</sup> from the QCSE.

The features observed in Fig. 12(a) have the general "derivative-type" shape expected of a discrete absorption feature. Such absorptions are apparent in Fig. 12(b), which shows the bias-induced change in transmission through the guide. In Fig. 13 we have converted our phase-shift and transmission data to changes in the effective index of refraction of the waveguide. Figure 13(a) shows the change in the real part of the guide index,  $\Delta n$ , and Fig. 13(b) shows the corresponding change in the imaginary part of the guide index,  $\Delta k$ . Figure 13(b) shows that the electro-absorption in the sample shows an exciton plus band-to-band character, but the magnitude of the absorption is too weak (and its dependence on wavelength is too strong) to be identified as the usual intra-well light-hole exciton associated with the QCSE. Note that the chirp parameter is strongly dependent on wavelength and bias in this structure, and regions favorable for practical applications in phase modulation ( $\Delta n/\Delta k > 20$ ) and intensity modulation ( $\Delta n/\Delta k < 2$ ) are readily found in Fig. 13. We observed an intensity modulation of 16:1 between 0 and 7.6 V reverse bias at a wavelength of 861 nm, with a corresponding chirp parameter  $\Delta n/\Delta k = 1.05$ .



(a)



(b)

FIG. 12. Measured phase shift (a) and intensity change (b) in sample 919 at four different TM-polarized laser wavelengths below the effective bandgap of the wide quantum well as a function of applied reverse bias.



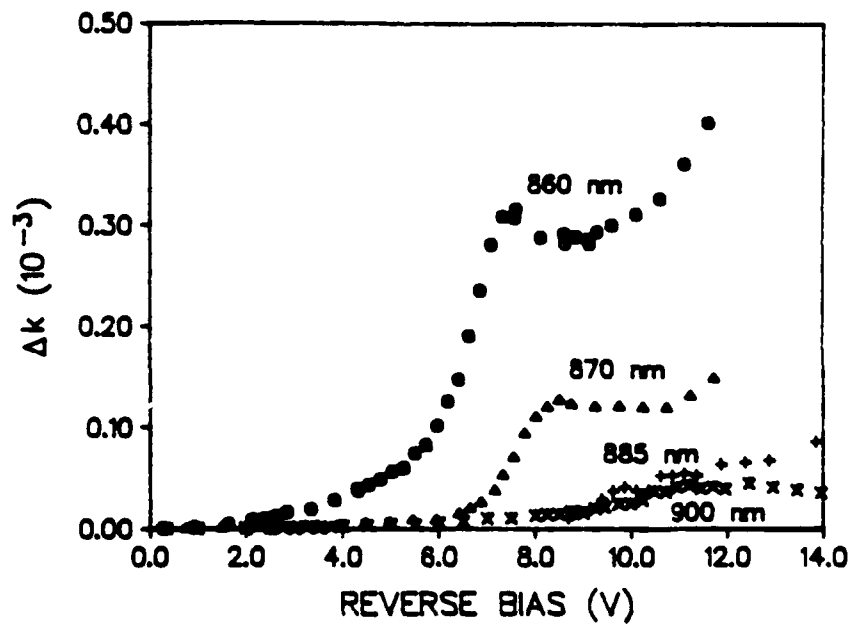
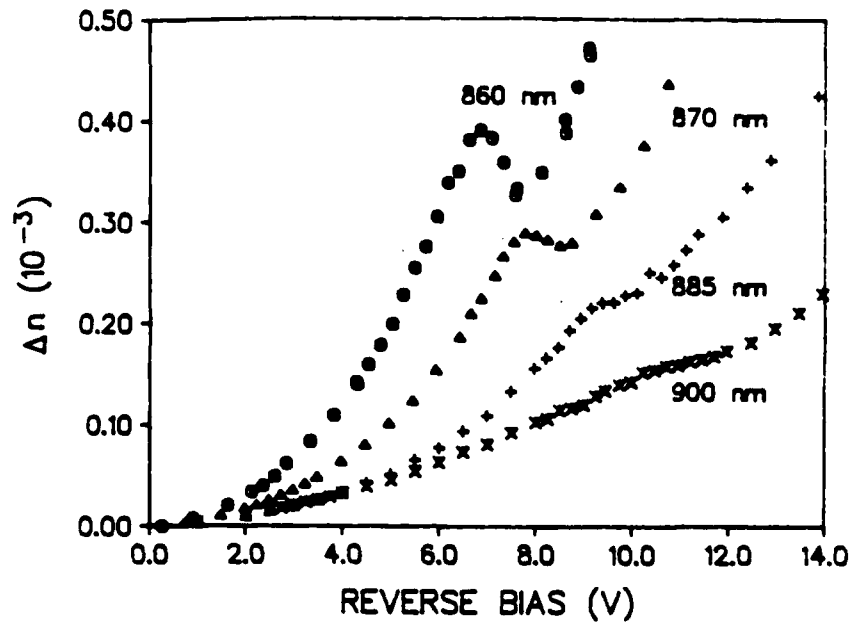


FIG. 13. Measured change in the real (a) and imaginary (b) part of the effective waveguide refractive index in sample 919 at four different TM-polarized laser wavelengths below the effective bandgap of the wide quantum well as a function of applied reverse bias.

The bias at which the absorptions are observed in Fig. 13 is a strong function of wavelength, and the apparent oscillator strength of the transition decreases with increasing laser wavelength. These observations are consistent with the hypothesis that the observed features are associated with the inter-well (wide-well hole to narrow-well electron) transition, confirming the theoretical prediction of a significant oscillator strength for this transition well beyond the avoided level crossing. At a given laser wavelength, the applied bias needed to bring this transition into coincidence with the laser line is much smaller than that needed to Stark shift the main wide-well transition into coincidence with the laser.

We devised a simple model of the coupled-well system that accurately reproduces the results of more sophisticated calculations.<sup>23</sup> We consider the interaction of the two isolated-well subbands through the tunnel barrier using the following Hamiltonian for the two-subband system:

$$H = H_0 + H_1 \quad . \quad (4)$$

In Eq. (4),  $H_0$  is the unperturbed Hamiltonian for the two isolated wells,

$$H_0 = E_w |w\rangle \langle w| + (E_n - eFd) |n\rangle \langle n| \quad , \quad (5)$$

where  $E_i$  and  $|i\rangle$  are the unperturbed energies and eigenstates of the isolated wells ( $i = w$  and  $n$  correspond to the wide and narrow wells) and  $d$  is the separation between well centers. (The origin is chosen at the center of the wide well, but dipole terms corresponding to the choice of origin are cancelled out in the total transition energy when the hole subband energy is added). Also in Eq. (4),  $H_1$  is the interaction Hamiltonian representing the well coupling,

$$H_1 = \frac{\Delta}{2} (|n\rangle \langle w| + |w\rangle \langle n|) \quad , \quad (6)$$

where  $\Delta$  is equal to the minimum splitting of the electron energy levels at resonance. The

eigenstate for the complete Hamiltonian is written as

$$|\psi\rangle = c_w |w\rangle + c_n |n\rangle, \quad (7)$$

and the eigenvalues and eigenstates of the full Hamiltonian, Eq. (4), are determined by solving  $H\psi = E\psi$  as a  $2 \times 2$  matrix equation. The unperturbed electron energies  $E_w$ ,  $E_n$  are determined by fitting single-band envelope-function calculations for the isolated wells to a parabolic form. (We also use a parabolic fit to the wide-well hole energies.) The coupling parameter  $\Delta$  can be obtained either from experimental data (e.g., low-temperature photocurrent data) or by performing a full envelope-function calculation for the coupled-well system.

Once the full eigenvalues and eigenstates are obtained, the electro-optical properties of the ACQW system are calculated by making a few simplifying assumptions. First, the overlaps between the wide-well hole subband and the two localized electron subbands are taken to be  $\langle h|w\rangle = 1$  and  $\langle h|n\rangle = 0$  for all values of the electric field. Thus, the oscillator strength for a given electron-hole transition is proportional to the magnitude of  $|c_w|^2$  for that transition. In this approximation, all the intensity in the inter-well transition comes from mixing the two electron subbands. Second, the excitons are assumed to have a Lorentzian line profile, with a half-width  $\Gamma_e$  that is independent of field. The oscillator strengths for the excitonic transitions are assumed to be proportional to the corresponding band-to-band transitions, and the exciton binding energies are assumed to be independent of field. The line shape for a band-to-band transition is given by the integral over energy of a Lorentzian:

$$\begin{aligned}
f(E) &= \frac{1}{\pi} \int_{-\infty}^E dE' \frac{\Gamma_b}{(E' - E_0)^2 + \Gamma_b^2} \\
&= \frac{1}{2} \left\{ 1 + \tan^{-1}[(E - E_0)/\Gamma_b] \right\} , \tag{8}
\end{aligned}$$

where  $E_0$  is the energy of the subband edge of interest and  $\Gamma_b$  is the Lorentzian half-width. Generally, we chose  $\Gamma_b = 2\Gamma_e$ . The choice of Lorentzian functions for the exciton line shape and in Eq. (8) tends to overestimate the amount of absorption well below the gap, but the details of the electro-refraction are not very sensitive to the choice. Since the absorption coefficient and the refractive index are related by a Kramers-Kronig transform, the change in refractive index is calculated for each exciton and each band-to-band transition by using the integral in Eq. (1), which can be performed analytically for both the band-to-band and excitonic functions.

Results of the calculations for the experimental sample are shown in Fig. 14, where we have chosen a light-hole exciton binding energy of 12 meV, an exciton half-width of 5 meV, and a minimum splitting  $\Delta$  of 9.7 meV (following the PC results of Section III.B). The electro-refraction is almost totally dominated by excitonic contributions; calculations performed without the band-to-band contribution to the index differed little from Fig. 14. Comparison of the electro-refraction calculations with the experimental result for  $\Delta n$  as a function of applied bias (Fig. 13) shows that the calculations agree at least semi-quantitatively with the data and support the suggested interpretation. The calculated results turn out to be somewhat sensitive to the choices of  $\Gamma_e$  and  $\Delta$ , and perhaps one could obtain better agreement by adjusting these parameters somewhat. However, considering that we have left out several effects (including field dependence of the exciton binding energy and width), the agreement is quite good.

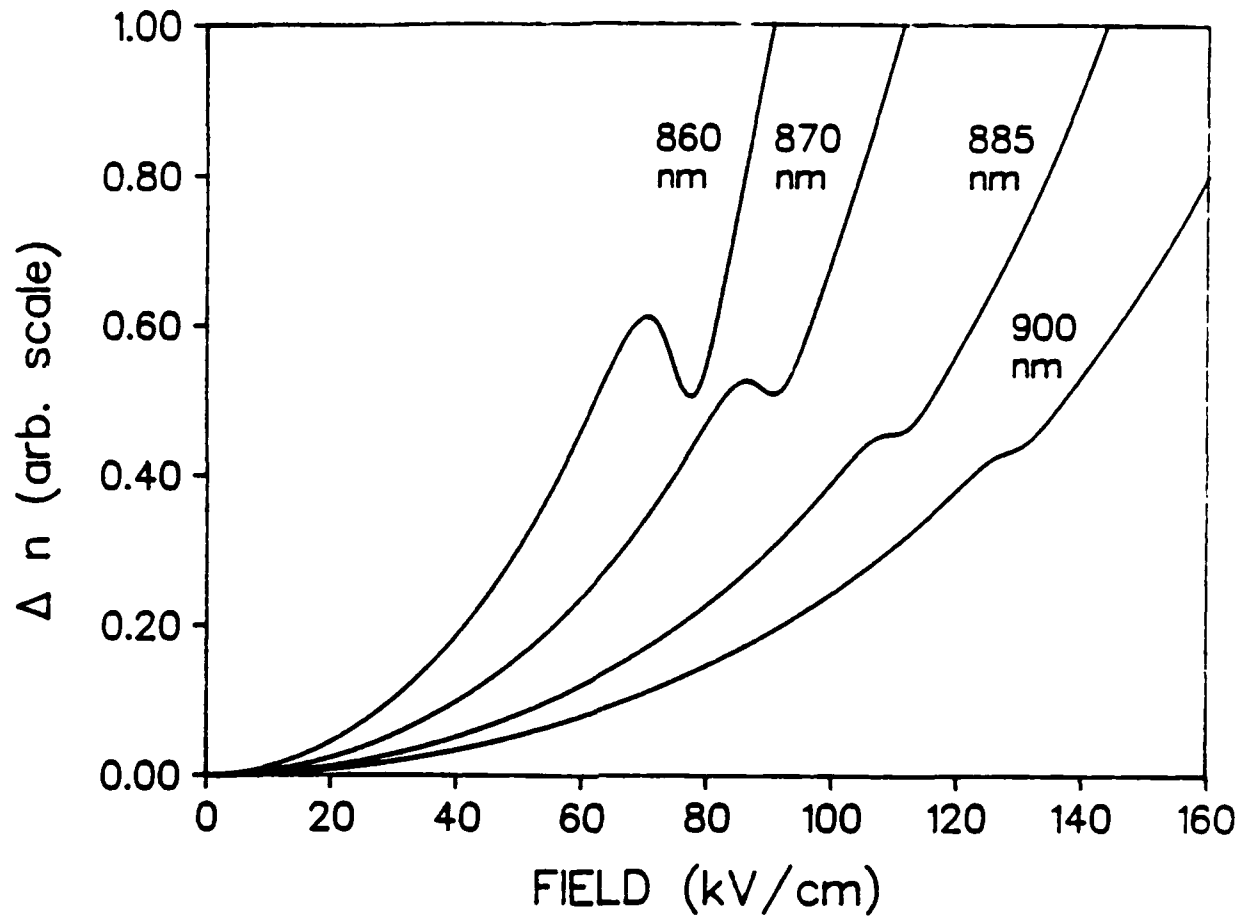


FIG. 14. Calculated change in the real part of the refractive index for sample 919 as a function of electric field for the four laser wavelengths used in the experiment. Calculations were performed assuming a light-hole exciton binding energy of 12 meV, an exciton half-width  $\Gamma_e$  of 5 meV, and a minimum splitting  $\Delta = 9.7$  meV of the two electron states.

As in the QCSE, the inter-well transition associated with the ACQW structure causes both a direct electro-absorption and a related electro-refractive effect. Both may be exploitable in electro-optic devices. This transition has two properties that are advantageous over the QCSE. First, the details of the transition are controlled by the geometry of the coupled-well system and as a result can be altered substantially by a simple change in the coupled-well structure. Second, for all voltages higher than that needed to bring the electron subbands into resonance, the energy of the transition is lower than that of the Stark-shifting wide-well transition. Thus, the inter-well transition causes electro-absorption and electro-refraction that are similar in nature to those caused by the QCSE, but they occur at lower applied voltages for operating wavelengths that are nominally well below the band edge of the quantum wells. Since the transition is spatially indirect, the presence of a large number of carriers can produce a depolarization field that would reduce the potential difference between the wells. As a result, as is analogous with a n-i-p-i device,<sup>33</sup> the inter-well transition may be optically controllable with above-bandgap radiation.

## IV. RESULTS FOR InGaAs/InAlAs STRUCTURES

### A. GROWTH OF InGaAs and InAlAs ON InP SUBSTRATES

In this section, we describe the steps taken to optimize the quality and reproducibility of InGaAs and InAlAs grown by MBE on InP substrates. This is the material system from which we fabricated MQW waveguides for intensity and phase modulators operating at 1.55  $\mu\text{m}$ . Since coming on line at the end of May 1988, our new Varian GEN-II MBE machine has been used extensively to grow InGaAs/InAlAs structures. It has many features that make it better suited to grow these materials than the Physical Electronics PHI-425B MBE machine used for the GaAs/AlGaAs growths. For example, the design of the substrate heater leads to a very uniform temperature distribution across the surface of the substrate. This is critical since the rate of In desorption from the wafer surface depends strongly on substrate temperature in the temperature range for which material quality is optimum. Consequently, if the substrate temperature were nonuniform, both the In mole fraction and the thicknesses of the InGaAs and InAlAs layers would vary considerably across the wafers. This was, in fact, the case in our preliminary growth studies of these compounds in the PHI machine.

In contrast to the PHI MBE, the Varian machine has a nude ion-gauge flux monitor mounted on the substrate holder that can be rotated into the substrate position and used to precisely set the beam fluxes of each of the group III constituents (In, Ga, Al) prior to conducting each day's growths. The most accurate and reproducible flux measurements were obtained by warming the group III cells up to growth temperature early each day and allowing them to stabilize for approximately two hours prior to conducting the flux measurements. The measurements were conducted in the absence of an  $\text{As}_4$  background pressure, i.e., the  $\text{As}_4$  cell was not warmed up until the measurements were complete. An

initial measurement was taken for each group III cell by opening its shutter and waiting several minutes until transients died out and the flux was truly stabilized. The measured flux was compared to the desired value, and an appropriate correction to each cell temperature was applied based on the result. After an additional 15-minute wait, the fluxes were measured again; this process was iterated until the desired fluxes were obtained for each constituent.

In order to obtain lattice match to InP substrates in the ternary semiconductors  $\text{In}_x\text{Ga}_{1-x}\text{As}$  and  $\text{In}_y\text{Al}_{1-y}\text{As}$ , the indium mole fractions must be maintained close to the lattice-match values ( $x=0.53$ ,  $y=0.52$ ) throughout the growth. If the In mole fractions deviate by more than a few percent from lattice match, the strain resulting from the lattice mismatch between the epilayer and the substrate will generate threading dislocations that can seriously degrade the electrical and optical quality of the material. Therefore, the ability to accurately provide absolute calibrations for each of the group III fluxes is essential.

We have developed a technique for absolute flux calibration that uses x-ray diffraction (XRD) measurements on superlattices (alternating layers of two different semiconductors) to calibrate the flux monitor for each group III cell. X-ray diffraction is commonly used to determine the lattice constant of homogeneous epilayers and to verify lattice-match to the substrate. Additional features (sidelobes) appear in the diffraction spectrum of a superlattice because the Bragg-reflection conditions can be satisfied by the periodicity of the superlattice. The separation (in angle) of the sidelobes from the atomic-lattice features depends inversely on the period of the superlattice and can be used as a very accurate measure of the sum of the thicknesses of the two constituents of the superlattice. The position of the atomic-lattice feature (which ideally coincides with the substrate feature) can be used to determine the relative concentrations of the group III



constituents. These two measurements give an accurate determination of the growth rates and, when compared with readings taken before the growth, serve to calibrate the flux monitor.

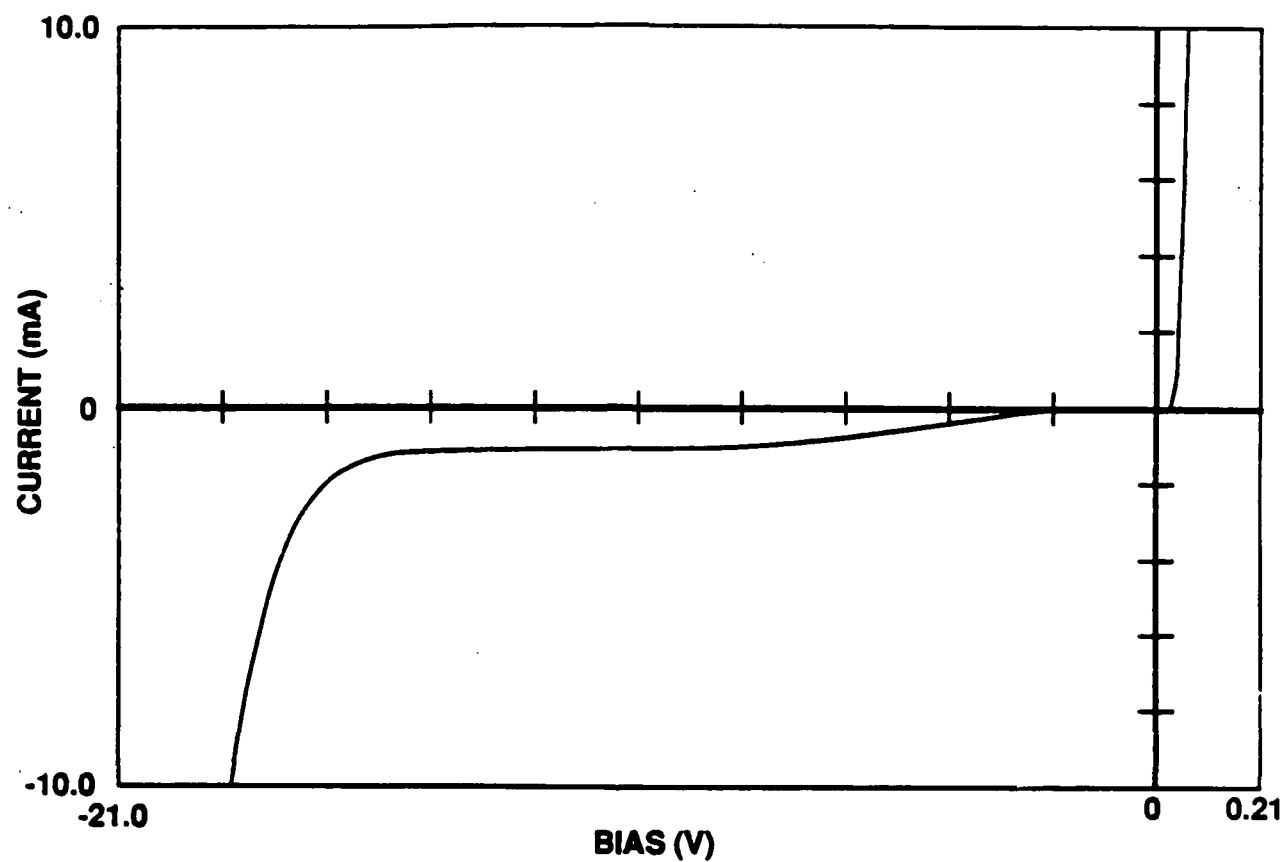
As applied to the InGaAs/InAlAs system on InP, our calibrations were obtained by growing single layers of InGaAs or InAlAs on InP and analyzing them using standard XRD techniques to obtain the In mole fraction in each compound. An additional InGaAs/InAlAs growth was then analyzed by XRD as discussed above to establish the overall growth rate. In practice, each of the InGaAs/InAlAs MQW samples grown for this contract contained a superlattice that was sufficiently thick to analyze using XRD. (This superlattice consisted of the MQW regions themselves for the samples characterized with photocurrent measurements and superlattice cladding layers for the waveguide samples.) Thus, we were able to monitor the absolute growth rate on a day-to-day basis while growing samples for the contract.

In addition to the stability and reproducibility of the group III beam fluxes and substrate temperature, the primary variables of interest in optimizing the quality of InGaAs and related compounds are the overall growth rate, the value of the growth temperature, and the ratio of the group V ( $As_4$ ) and group III fluxes. We narrowed considerably the range of choices for each of these quantities by relying on published results<sup>34</sup> concerning growth of these compounds. Our initial efforts in this material system were conducted on the PHI MBE. During this time we conducted experiments to determine the range of good growth temperatures by growing a series of 1- $\mu$ m-thick InGaAs layers and characterizing them by measuring the full width at half-maximum of the epilayer Bragg peak obtained via XRD. In this way, we determined that good quality epilayers could be obtained consistently by growing at a substrate temperature of 520°C. The growth rate for films grown on the PHI machine was 0.6-0.8  $\mu$ m/hr with an  $As_2$  source. We tried

growing our initial films on the Varian MBE at 1.2  $\mu\text{m/hr}$  with an  $\text{As}_4$  source and their quality was even better than those obtained on the PHI MBE. With the  $\text{As}_4$  source, we set the group V/group III ratio in the range of 5:1 to 6:1, consistent with previous reports.<sup>34</sup>

The morphology of films grown under these conditions was consistently excellent. Hall effect measurements showed that the background carrier concentration in the InGaAs layers was  $5\text{-}7 \times 10^{15}/\text{cm}^3$ , which is excellent for this system. Hall measurements on the InAlAs films showed complete depletion of 1- $\mu\text{m}$ -thick films, indicating either a very low background density ( $< 10^{15}$ ) or semi-insulating films. Rather than characterize the optical quality using PL as we attempted to do in our earlier efforts to grow good InGaAs, we decided to use the quality of the quantum-well structures themselves as the most relevant indicator, with the intent of changing the growth conditions if poor results were obtained. This turned out to be unnecessary.

The MQW samples grown for the contract contain quantum wells embedded in a p-i-n diode, which must have low leakage currents for reverse biases of 10-20 V. In order to establish the suitability of our InGaAs/InAlAs material for such applications, we grew two InGaAs and two InAlAs p-i-n diodes (with no quantum wells) with the In mole fraction within 0.04 of the lattice-match values. The layer thicknesses were 0.25- $\mu\text{m}$  n-type, 0.5- $\mu\text{m}$  intrinsic, and 0.25- $\mu\text{m}$  p-type. These samples were processed into 250- $\mu\text{m}$  diameter mesas with ohmic contacts made to the n-type substrate (Au/Sn/Au, annealed at 310°C for 30 s) and to the p-type mesa tops (Au/Cr/Au, unannealed). Figure 15 shows the current-vs-voltage (I-V) characteristic for one of the InGaAs diodes. The forward-bias characteristic is excellent. However, for reverse biases larger than about 2 V, the I-V characteristic exhibits a plateau in the leakage current (saturating at about 1 mA). Reverse-bias breakdown occurs at 16-17 V. We do not know the origin of the plateau at



L894-7092-1

FIG. 15. Current-voltage (I-V) characteristic for an InGaAs p-i-n diode grown on InP. Note its large reverse-bias leakage current.

this time. Figure 16 shows the I-V characteristic for one of the InAlAs diodes, which shows good forward- and reverse-bias characteristics. (Reverse-bias leakage currents are negligible until breakdown at 30-32 V). Because the intrinsic regions of the waveguide phase-shifter samples are composed primarily of InAlAs (with a substantial amount of InGaAs only in the quantum-well layers), we expected that Fig. 16 would be more representative of the I-V characteristics of the MQW waveguides. This expectation was borne out by the actual results obtained in all our InGaAs/InAlAs MQW samples.

## B. PHOTOCURRENT STUDIES OF InGaAs/InAlGaAs ACQW SAMPLES

Having determined optimum growth conditions for single epilayers of InGaAs and InAlAs on InP on the new MBE system, we grew a few structures containing many (40-60) quantum wells. The undoped QW structures in these samples are relatively thick (by the standards of the GaAs/AlGaAs samples discussed above) and could (in principle) be plagued with the same problems (nonlinearities, nonuniform fields) discussed in Sections II and III. Our intent was to characterize the quality of the InGaAs quantum wells at zero field (room-temperature exciton peak width, for example) and also to obtain direct experimental information on the effective bandgap (energy of the  $h_1e_1$  transition) of the QW system for typical well widths. The structures were grown in p-i-n diodes to permit us to determine the electrical diode characteristics, in anticipation of growing QW waveguides with much thinner intrinsic regions.

Nevertheless, these samples turned out to be among the best InGaAs structures grown for the contract. In spite of the relatively thick intrinsic regions in the samples, the quantum-well features remained sharp over a wide range of applied biases, as determined by room- and low-temperature PC measurements, and there was no evidence of significant nonuniformities in the fields. The low background doping in these samples

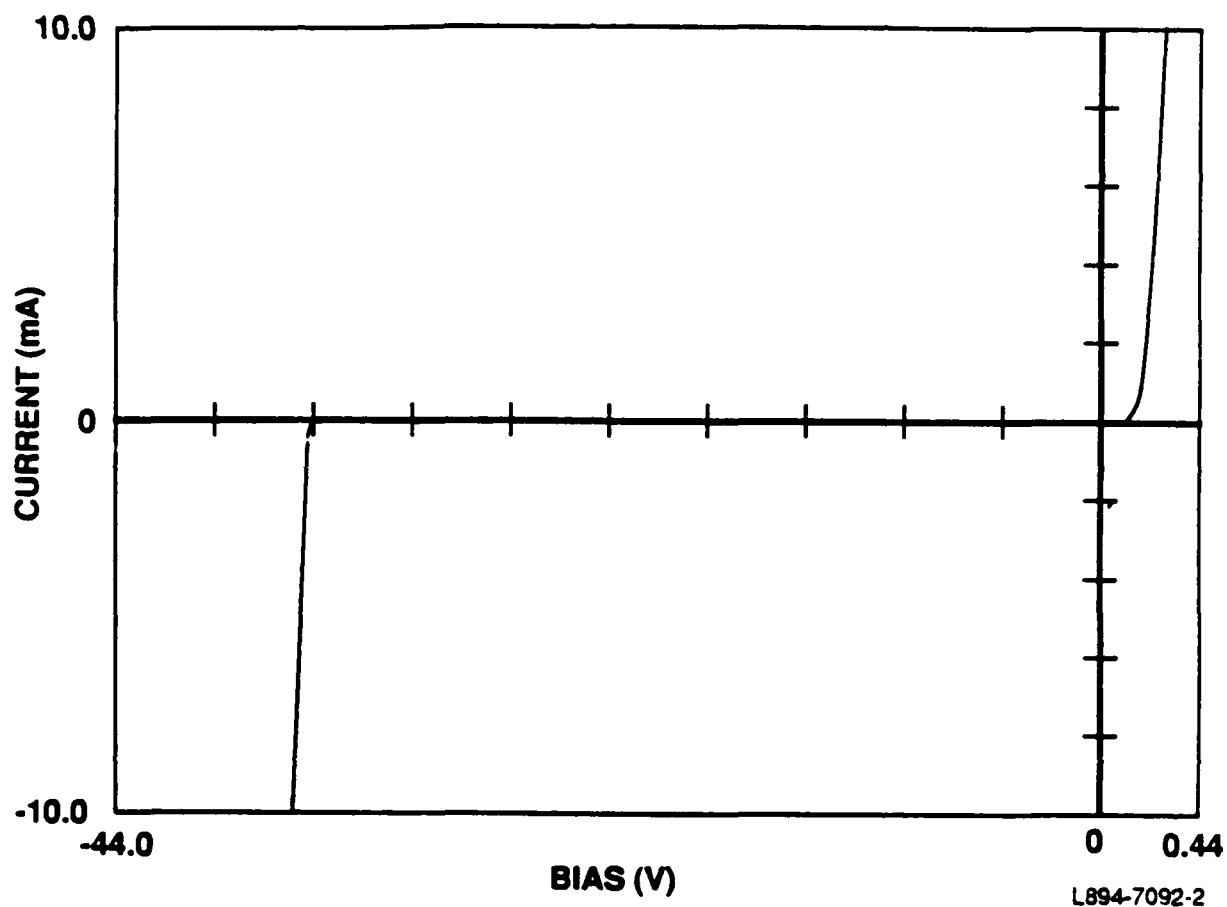
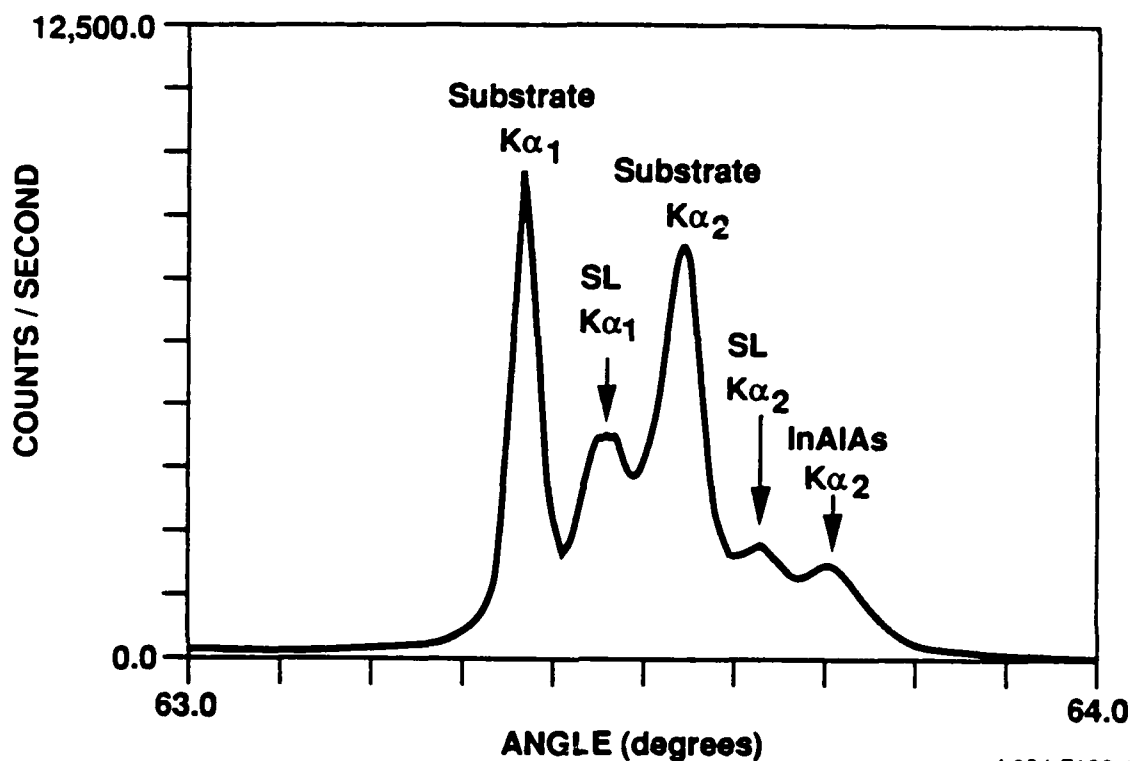


FIG. 16. Current-voltage (I-V) characteristic for an InAlAs p-i-n diode grown on InP. This sample (and the MQW samples discussed later) does not have the leakage-current problem shown in Fig. 15.

(which is most likely responsible for the field uniformity) is the result of two factors: (a) the growth chamber of our new MBE system is extremely clean (base pressure  $< 3 \times 10^{-10}$  Torr with the As cell cold) and therefore there is little carbon available for incorporation during growth, and (b) we used an ultra-pure In source (99.99995 % purity). In earlier growths on our old MBE system, a less pure In source was used that was found to be contaminated with sulfur, which is an n-type dopant in InGaAs. Alternative explanations for the lack of substantial background doping are that (a) deep levels are trapping the free carriers or (b) there is accidental cancellation of p- and n-type doping arising from C and S, respectively. We believe that neither of these alternatives is consistent with the good quality of the room- and low-temperature excitons observed in the samples, however.

Apparently it is possible to obtain excellent quantum-well structures with a degree of lattice mismatch that we originally considered unacceptable. In Fig. 17 we show a single-crystal XRD spectrum (004 reflection) for sample EO-72 (described below) in the vicinity of the InP substrate peak. The three sets of peaks shown correspond to the InP substrate, the QW structure itself (with the observed peaks being associated with a weighted average of the InGaAs and InAlAs lattice constants), and the thick InAlAs buffer. The compositional mismatch of the InAlAs relative to the InP substrate is about 3% (In lean), whereas the InGaAs is lattice matched. (The InGaAs lattice constant was determined primarily from a companion, thick InGaAs sample grown following the QW sample, but it can also be deduced from the effective lattice constant of the QWs determined from Fig. 17.)

By studying bias-induced shifts in both coupled and uncoupled well structures with room- and low-temperature PC spectroscopy, we have shown that ACQWs can overcome many of the limitations<sup>36</sup> of the QCSE as applied to phase and intensity modulators at the optimum fiber-optic wavelengths, 1.3 and 1.55  $\mu\text{m}$ . The primary difficulty in



L894-7129-1

FIG. 17. Single-crystal x-ray diffraction spectrum of an InGaAs/InAlAs ACQW sample (EO-72) in the vicinity of the [004] InP substrate reflection. Three sets of peaks are observed, corresponding to the substrate, the SL region (which for this sample is the coupled-quantum-well region), and a thick InAlAs buffer. Despite the somewhat large lattice mismatches in this sample, its optical quality is excellent.

applying the QCSE to such devices is that its strength depends strongly on the widths of the quantum wells and is very small for the relatively thin ( $\sim 3\text{-}8\text{ nm}$ ) wells required for operation at these wavelengths. Our results<sup>36</sup> show that the shifts in the excitonic absorption peaks in the ACQW structure are large even for low biases.

The InGaAs/InAlAs MQW samples studied for the contract were grown on  $n^+$  substrates. The layer sequence for the samples, starting from the InP substrate, is as follows:  $0.35\text{-}\mu\text{m}$   $n^+$  ( $\sim 2 \times 10^{18}/\text{cm}^3$  Si) InAlAs,  $0.15\text{-}\mu\text{m}$  undoped InAlAs,  $0.7\text{-}\mu\text{m}$  undoped MQW region,  $0.15\text{-}\mu\text{m}$  undoped InAlAs,  $0.2\text{-}\mu\text{m}$   $p^+$  ( $\sim 2 \times 10^{18}/\text{cm}^3$  Be), and a  $20\text{-nm}$   $p^+$  InGaAs contact layer. The total thickness of the intrinsic region is  $1.0\text{ }\mu\text{m}$ . The control sample's MQW region has 40 periods of a  $7.5\text{-nm}$  InGaAs well plus a  $10.0\text{-nm}$  InAlAs barrier (sample EO-64 in Appendix A). For the ACQW sample (EO-72), the MQW region consists of 29 periods of the following structure: a  $5.0\text{-nm}$  InGaAs well, a  $1.6\text{-nm}$  InAlAs barrier, a  $7.5\text{-nm}$  InGaAs well, and a  $10.0\text{-nm}$  InAlAs barrier.

Pieces of the wafer were polished mechanically on the back to remove the indium-mounting solder and to provide a smooth surface onto which an n-type (Au/Sn/Au) ohmic contact was evaporated and annealed (by rapid thermal annealing) at  $310\text{ }^\circ\text{C}$  for 30 s. An array of non-annealed p-type (Au/Cr/Au) ring contacts was evaporated onto the top surface, and  $250\text{-}\mu\text{m}$ -diameter mesas were defined by etching down to the InP substrate with a 9:1:1 mixture of  $\text{H}_2\text{O}$ ,  $\text{H}_2\text{O}_2$ , and  $\text{H}_3\text{PO}_4$ , which is a highly selective etch for both InGaAs and InAlAs over InP.

The photocurrent experiments were performed as described previously, except that the spectrometer was purged with  $\text{N}_2$  gas to minimize the effects of atmospheric absorption lines that occur at about  $1.4\text{-}\mu\text{m}$  wavelength. For the low-temperature measurements, where the primary absorption lines of interest overlap the atmospheric absorptions, we divided the recorded photocurrent spectra by the spectrum of a Ge photodiode



measured with the same apparatus.

Figure 18 shows the room-temperature PC spectra of the control sample (EO-64) for reverse biases of 0, 3, 6, and 9 V. The "noise" at about 0.9 eV arises from the atmospheric absorptions discussed above. Note that the  $h_1e_1$  (a) and  $l_1e_1$  excitons (b) exhibit small Stark shifts that vary quadratically with applied bias. The magnitudes of the observed shifts in this sample are consistent with single-band envelope-function calculations, indicating high-quality quantum wells with low deep-level and background doping densities.<sup>35</sup>

In Fig. 19, we show the room-temperature PC spectra for the ACQW sample (EO-72) at the same biases as in Fig. 18. Because of the thin barrier, the coupling in this sample is very strong, and small changes in the applied bias produce significant changes in the photocurrent spectra. For example, at 3-V reverse bias, the  $h_1e_1$  exciton is shifted by almost 4 meV from its zero-bias energy, and a new transition is seen at about 0.88 eV. The resonance and avoided-level crossing of the  $e_1$  and  $e_2$  electron subbands occurs at about 5-V reverse bias. Beyond resonance, the inter-well transition discussed in Section III persists over a wide range of applied biases and is easily observable at room temperature [see, e.g., the shoulder labeled (a) in the 9-V spectrum of Fig. 19], which has shifted by about 30 meV from its zero-bias energy. Comparison of Figs. 18 and 19 clearly shows that the features observed in the ACQW sample arise from coupling between the wells. (Note that the zero-bias heavy-hole peak occurs at slightly lower energy in sample EO-64 than in sample EO-72. This discrepancy can be accounted for by a difference in the In mole fraction of 0.015 in the InGaAs layers of the two samples.)

Figure 20 shows the low-temperature (8 K) PC spectra of sample EO-72 for applied reverse biases of 0, 3.5, 5, 6.5, and 10 V. Dramatic effects of level splittings associated with the coupling between quantum wells can be seen at low temperature, particularly

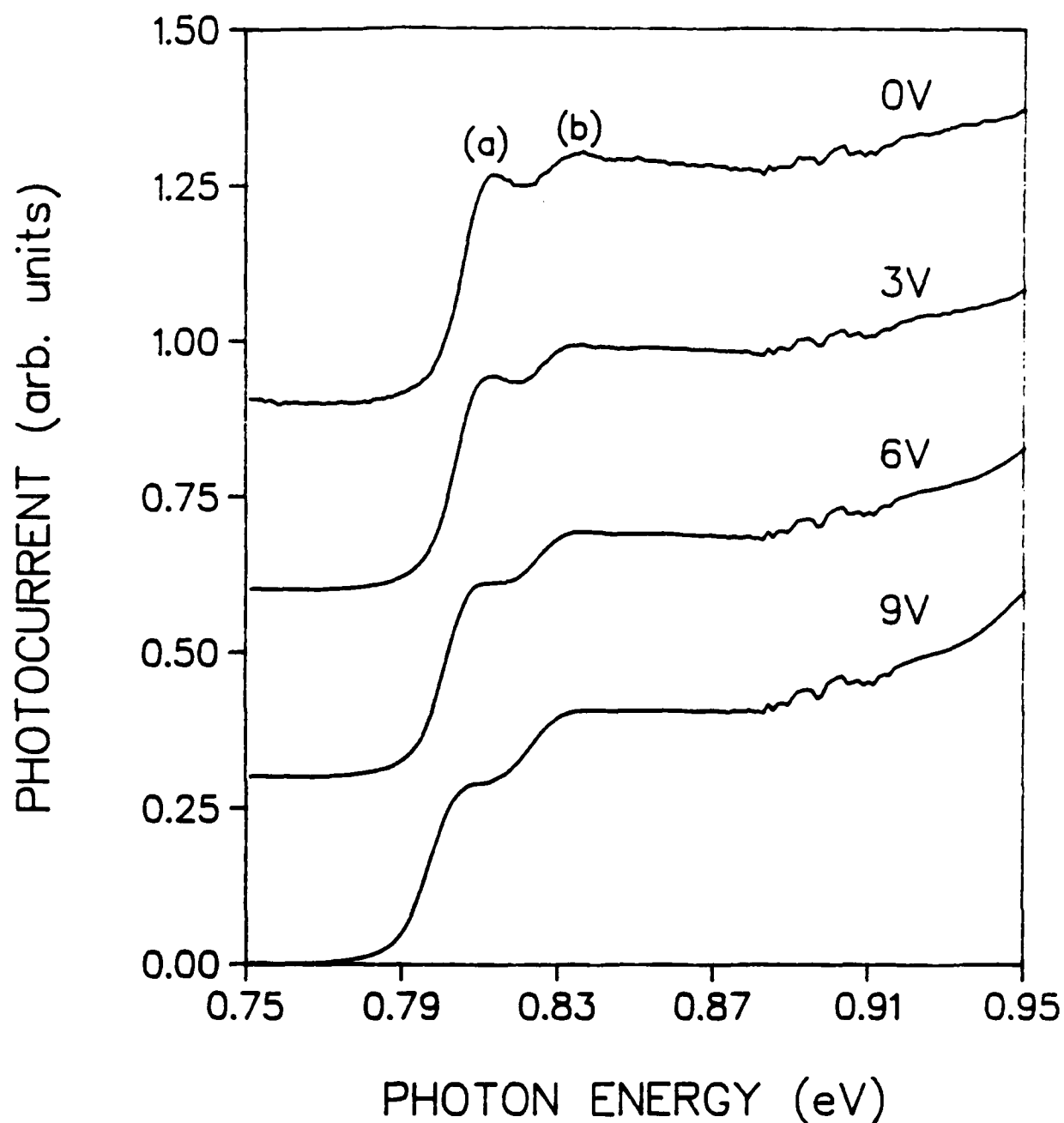


FIG. 18. Room-temperature photocurrent spectra of a control sample (sample EO-64) containing 40 periods of 7.5-nm InGaAs quantum wells separated by 10.0-nm InAlAs barriers, for several values of reverse bias. Transitions are labeled as follows: (a) -  $h_1e_1$  and (b) -  $l_1e_1$ . The "noise" in the spectra at about 0.9 eV is due to atmospheric absorption.

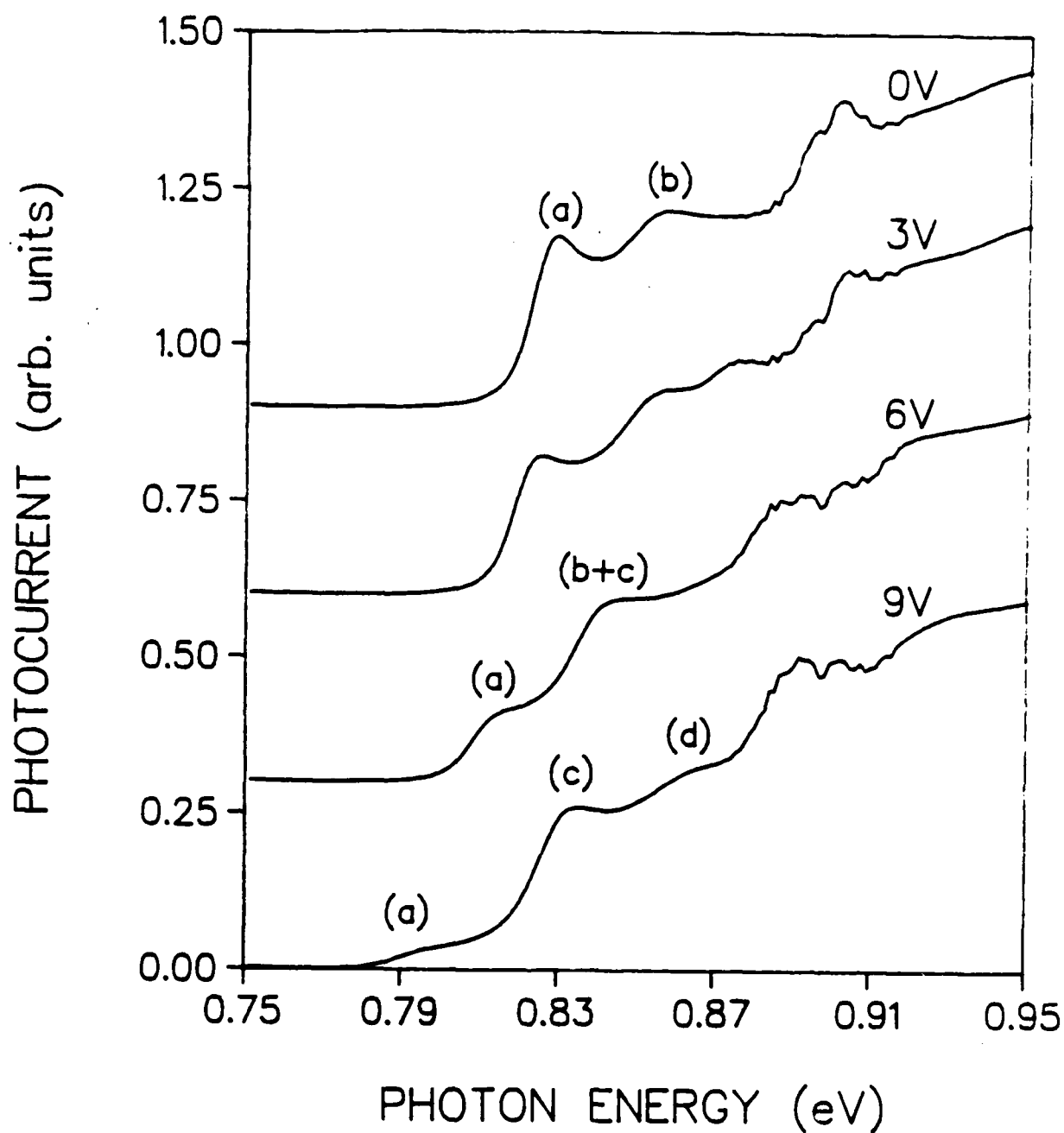


FIG. 19. Room-temperature photocurrent spectra of an ACQW sample (EO-72) containing 29 periods of 7.5- and 5.0-nm InGaAs quantum wells coupled by a 1.6-nm InAlAs barrier, for several values of reverse bias. The transitions are labeled as in Fig. 18, with the addition of (c) -  $h_1e_2$  and (d) -  $l_1e_2$ . Beyond resonance,  $h_1e_1$  is an inter-well transition.

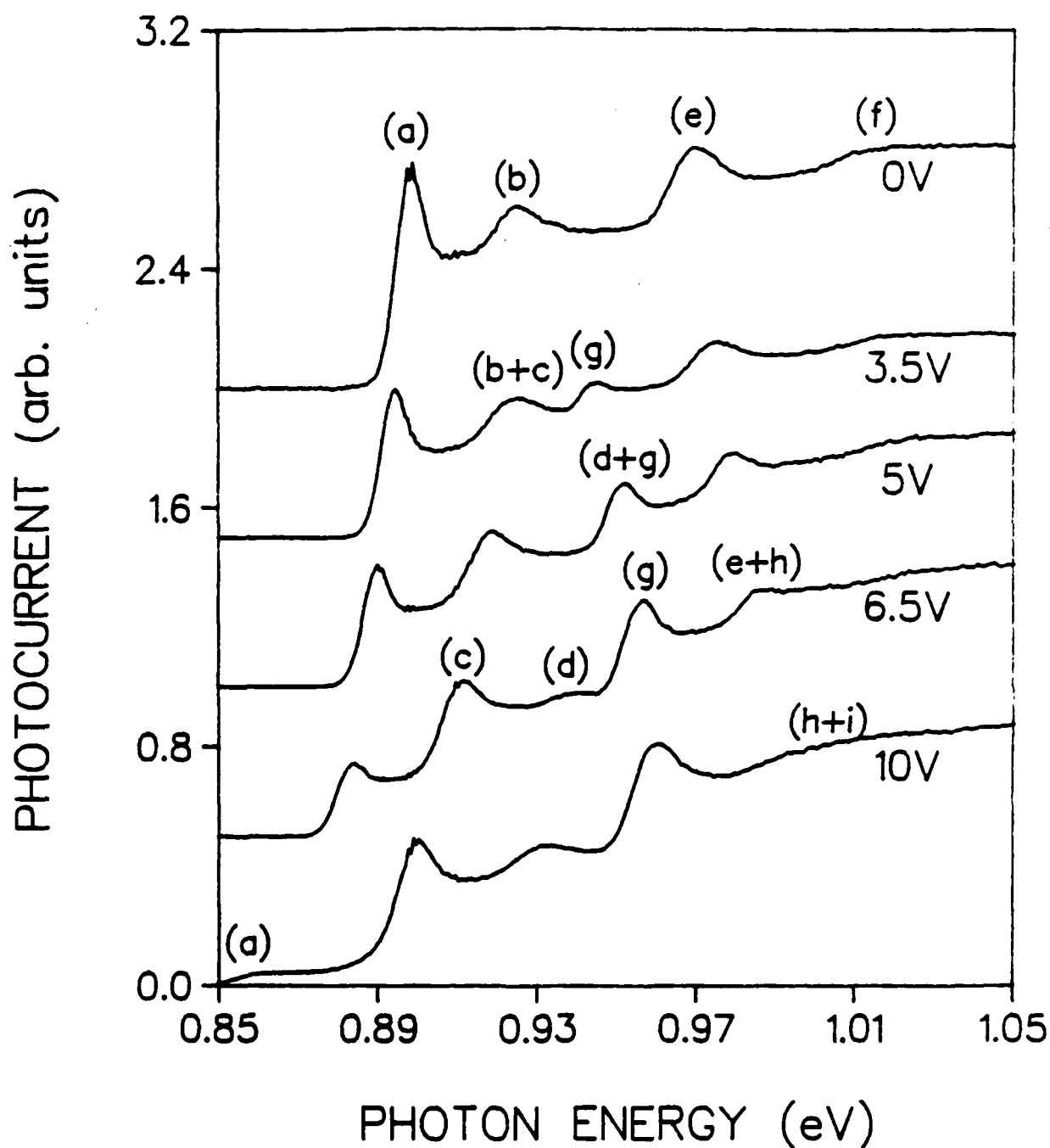


FIG. 20. Low-temperature (8 K) photocurrent spectra of sample EO-72 for several values of reverse bias. The transitions are labeled as in Figs. 18 and 19, with the addition of (e) -  $h_2e_2$ , (f) -  $l_2e_2$ , (g) -  $h_2e_1$ , (h) -  $l_2e_1$ , and (i) -  $l_3e_1$ .

near the resonance field (see, e.g., the 5-V spectrum in Fig. 20). Beyond resonance, the inter-well transition,  $h_1e_1$ , is the lowest-energy optical transition supported by the system, and it can be observed for biases well beyond resonance (see, e.g., the 10-V spectrum in Fig. 20).

Figure 21 shows the peak energies (symbols) of several low-temperature excitonic transitions as a function of applied bias. The solid (heavy holes) and dashed (light holes) lines show the calculated energies of transitions that are expected to have significant oscillator strengths in the 0.8-to-1.05-eV range in the ACQW system. The following material parameters were assumed for the calculations:<sup>36</sup> for InGaAs,  $m_e = 0.041$ ,  $m_{lh} = 0.0516$ ,  $m_{hh} = 0.377$ ; for InAlAs,  $m_e = 0.075$ ,  $m_{lh} = 0.085$ , and  $m_{hh} = 0.57$ . The valence- and conduction-band offsets were taken as 224 and 523 meV, respectively. In the calculations, the relationship between electric field and applied bias is determined by assuming a built-in potential of 0.6 V (determined from room-temperature capacitance-voltage measurements) and a total intrinsic-layer thickness of 1.0  $\mu\text{m}$ .

A brief digression on the theoretical calculations is in order here. The original theoretical calculations performed on the InGaAs system (and for all the GaAs structures discussed in Section III) assumed that the observed energy levels in the system corresponded to true bound states, i.e., that the electron and hole wave-functions decayed exponentially away from the quantum wells. In reality, as soon as a field is applied, the quantum-well subbands are no longer bound states since there is a finite probability of field-assisted tunneling out of the quantum wells and into the continuum. Previously this assumption caused no problems in practice, since the tunneling rate was very small and the quantum-well subbands are "quasi-bound" states. However, our first calculations for the InGaAs systems showed significant disagreement with experiment, particularly for the excited light-hole subbands at high reverse biases. We resolved the problem by using a

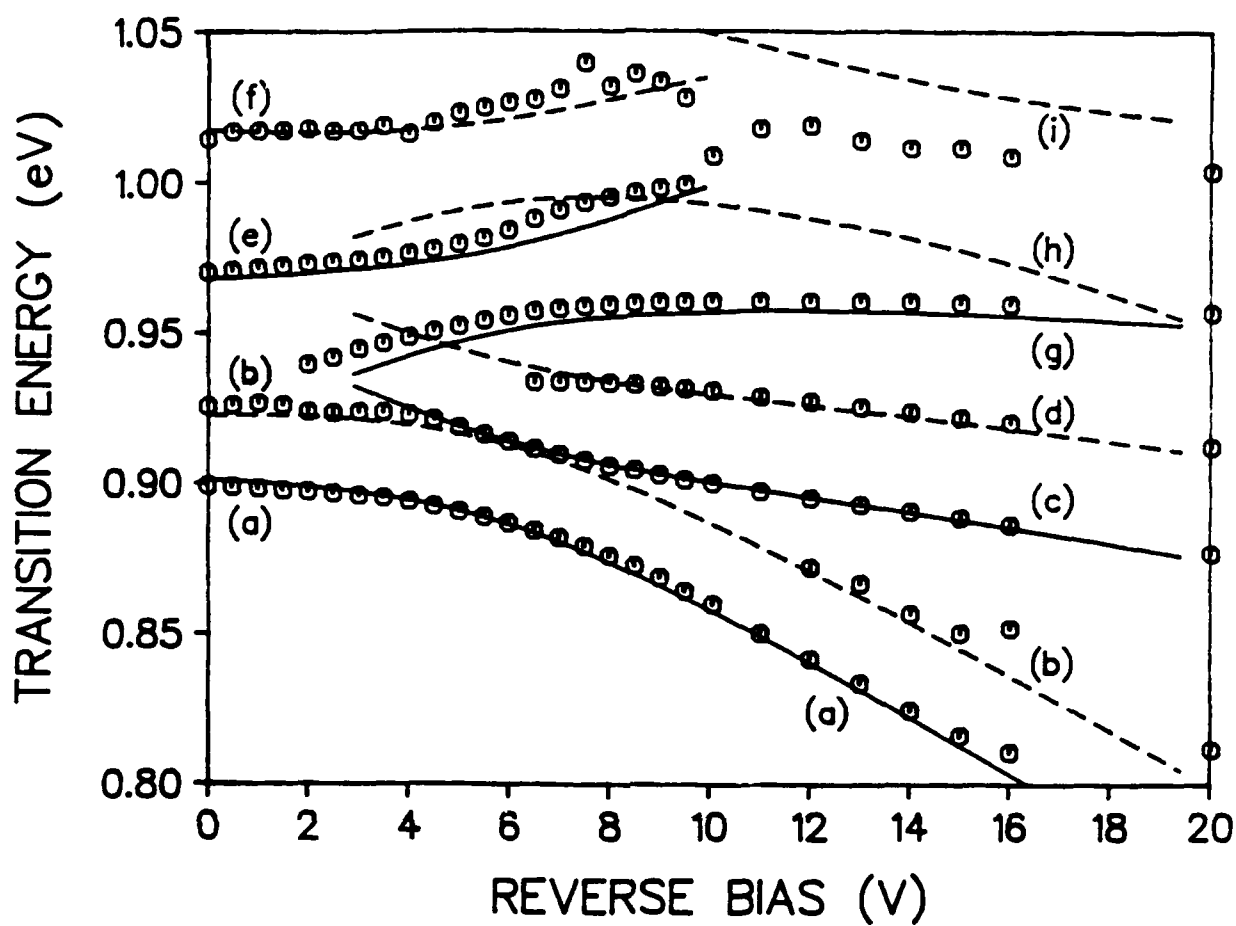


FIG. 21. Calculated and observed (at 8 K) transition energies as functions of applied reverse bias for sample EO-72. Transitions are labeled as in Figs. 18-20. Solid lines indicate heavy-hole transitions, and dashed lines are light-hole transitions.

method in which the quantum-well system is treated as a scattering problem.<sup>37</sup> Specifically, one looks for resonances in the phase shift in the scattered wave resulting when an electron (or hole) is incident on the quantum-well system. This method was used to obtain the theoretical results shown in Fig. 20. It agrees with the bound-state method when field-assisted tunneling is small, and has the additional advantage of giving the width of the scattering resonance (and therefore the tunneling contribution to the lifetime) when tunneling is non-negligible.

The electron subbands  $e_1$  and  $e_2$  come into resonance at about 5-V reverse bias, and transitions between the isolated heavy-hole subbands  $h_1$  and  $h_2$  (localized in the wide and narrow wells, respectively) to this coupled pair are apparent over a wide range of biases in Fig. 21. We could not follow the corresponding light-hole transitions over the entire bias range since these transitions are weaker and broader than the heavy-hole transitions. Beyond the electron-subband resonance, we predict an avoided-level crossing of the  $l_2$  and  $l_3$  hole subbands (at about 12-14 V), but the experimentally observed feature in this region is very broad and cannot be resolved into two transitions (see the feature labeled (h+i) in the 10-V spectrum in Fig. 20). Agreement between theory and experiment is entirely satisfactory, considering that the material parameters are not as well established for the InGaAs/InAlAs system as for the GaAs/AlGaAs system. Calculations (not shown) for the higher-energy transitions of the ACQW system do not agree as well with the experimental data (probably because we have neglected nonparabolicity in the conduction band), and so positive identification of these transitions is not possible at present.

To summarize our work on photocurrent spectroscopy in the InGaAs/InAlAs quantum-well system, we have shown that it is possible to obtain large shifts in the energies of excitonic transitions in ACQW coupled-quantum-well structures containing relatively thin wells, in which the normal QCSE is weak. Our results for the energies of

several excitonic transitions involving the coupled pair of electron subbands associated with the two wells are in excellent agreement with calculations performed using a scattering phase-shift method. This agreement gave us confidence in the use of our theoretical models to design InGaAs/InAlAs ACQW waveguides that, as we show below, produce significantly enhanced optical intensity and phase modulation in comparison with uncoupled-well modulators based on the QCSE.

### C. ELECTRO-ABSORPTION AND ELECTRO-REFRACTION IN InGaAs/InAlAs ACQW WAVEGUIDES

Previous work on long-wavelength quantum-well electro-optic modulators indicated much more promising results for InGaAs/InP than for InGaAs/InAlAs structures. Electro-absorption data<sup>38</sup> for the InGaAs/InAlAs waveguide structures showed a very small QCSE and substantial broadening of the excitonic transitions, attributed to a high background impurity concentration. Consequently, the observed phase shifts in InGaAs/InAlAs quantum-well waveguides were relatively weak,<sup>39</sup> and their dependence on bias was inconsistent with theoretical expectations based on the QCSE. On the other hand, work on the InGaAs/InP MQW system has shown effective phase modulation based on the QCSE.<sup>40,41</sup> In this latter work, phase-shift measurements were made with light propagating normal to the MQW layers in samples containing 3-nm wells<sup>40</sup> and 10-nm wells.<sup>41</sup> In the 3-nm-well sample, the operating wavelength was 1.5  $\mu\text{m}$ , but the magnitude of the QCSE and the corresponding electro-refraction were small, as expected from the narrow quantum wells. Large electro-refraction was observed in the 10-nm-well sample, although in this case the operating wavelength was 1.7  $\mu\text{m}$ .

As a result of our work on the contract, we can now show<sup>42</sup> that (a) it is possible to obtain electro-absorption and electro-refraction effects in InGaAs/InAlAs MQW



structures that are in good agreement with theoretical predictions, and (b) the use of ACQW structures in this material system leads to substantial improvements in the phase and intensity modulation characteristics observed in the wavelength region of interest for fiber-optic applications. We attribute the former to several factors (discussed in detail above), primarily the use of an ultra-high-purity In source and the ability to reproducibly attain optimum growth conditions. As a result, we have been able to reproducibly grow InGaAs/InAlAs MQW waveguide structures with well-defined room-temperature excitons and low concentrations of background impurities. As we show below, the use of ACQW structures allows us to obtain substantial shifts in the excitonic absorption features in a wavelength range favorable for operation of devices at 1.55  $\mu\text{m}$ . This is not possible for QCSE-based devices, since the well widths required for operation at 1.55  $\mu\text{m}$  are too small to obtain a substantial QCSE.

The samples grown for waveguide electro-absorption and electro-refraction studies contain the following layer sequence, grown on  $n^+$  InP substrates: a 0.65- $\mu\text{m}$   $n^+$  superlattice, consisting of 65 periods of 8.5-nm InAlAs and 1.5-nm InGaAs layers; a 0.35- $\mu\text{m}$  undoped superlattice; a 0.3- $\mu\text{m}$  MQW region; another 0.35- $\mu\text{m}$  undoped superlattice, a 0.65- $\mu\text{m}$   $p^+$  superlattice, and a 20-nm  $p^+$  InGaAs contact layer. Thus, the waveguides have a 0.3- $\mu\text{m}$  core with 1.0- $\mu\text{m}$  cladding on either side. For the present studies, four ACQW waveguides were grown (EO-74, EO-75, EO-76, and EO-79); EO-75 was chosen for detailed studies since its layers were closest to lattice match with the InP substrate, although differences in optical quality among the four samples were minimal. In EO-79, the superlattice cladding was replaced with thick InAlAs, but its doping profile was the same as the other samples, and its optical properties were very similar. In the ACQW samples, the MQW region consisted of 13 periods of a 5.0-nm InGaAs well, a 1.6-nm InAlAs barrier, a 7.5-nm well, and a 10.0-nm InAlAs layer separating well pairs. The ordering of the wells is such that an applied reverse bias brings the lowest electron subbands of

the two wells through resonance. A control sample, EO-77, was grown, which contained only uncoupled 7.5-nm wells with 16.6-nm barriers and with the same number of periods as the ACQW samples. The intrinsic region was 1.0- $\mu\text{m}$  thick for all the waveguide samples.

After growth, the samples were processed into slab waveguides as follows. The substrate was first thinned to approximately 80  $\mu\text{m}$ , and a blanket n-type ohmic contact was deposited onto the bottom surface and annealed. An array of 200- $\mu\text{m}$  outer-diameter p-type (Au/Cr/Au) ring contacts was evaporated onto the upper surface. A uniform layer of photoresist was spun onto the surface, and 250- $\mu\text{m}$ -wide mesa stripes were defined (with the contact rings centered on the stripes) using photolithography and chemical etching. The material was cleaved to form bars with facet-to-facet spacings ranging from 250 to 1000  $\mu\text{m}$ . The top-side ring contacts allowed us to perform normal-incidence photocurrent measurements and waveguide measurements on the same sample.

Photocurrent measurements were performed at room temperature to confirm the good optical quality of the samples and to verify that phenomena observed previously (see the discussion of samples EO-64 and EO-72 in Section IV.B above) also occur in the present samples. In the photocurrent spectra of sample EO-77 (the control sample containing uncoupled 7.5-nm wells) at zero bias and at a bias of 6 V (Fig. 22), the QCSE observed is similar to that observed in EO-64 earlier. In the photocurrent spectra at the same biases for the ACQW sample, EO-75 (Fig. 23), the shift of the  $h_1e_1$  exciton is much larger due to the coupling between the 7.5- and 5.0-nm wells. At 6 V, the sample is biased slightly beyond resonance, so the  $h_2e_1$  transition is comparable in strength to the  $h_1e_1$  transition. In the photocurrent spectra shown here, Fabry-Perot fringes appear that arise from multiple reflections from the front and back of the samples. The observed fringe spacing is consistent with the 80- $\mu\text{m}$  thickness of the present samples. They were

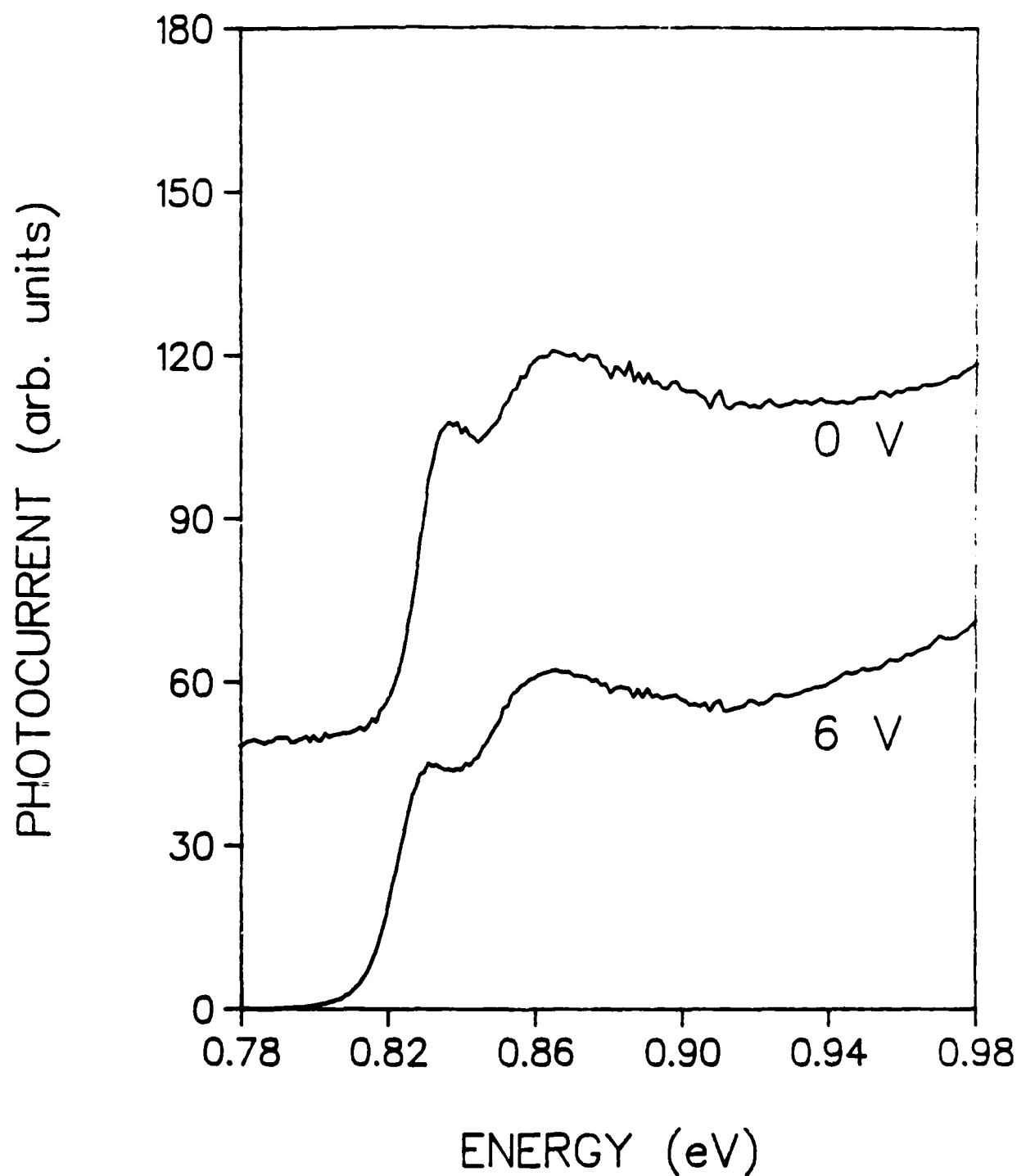


FIG. 22. Room-temperature photocurrent spectra of an InGaAs/InAlAs MQW waveguide sample (EO-77) containing only uncoupled 7.5-nm quantum wells at 0 V and 6 V reverse bias.

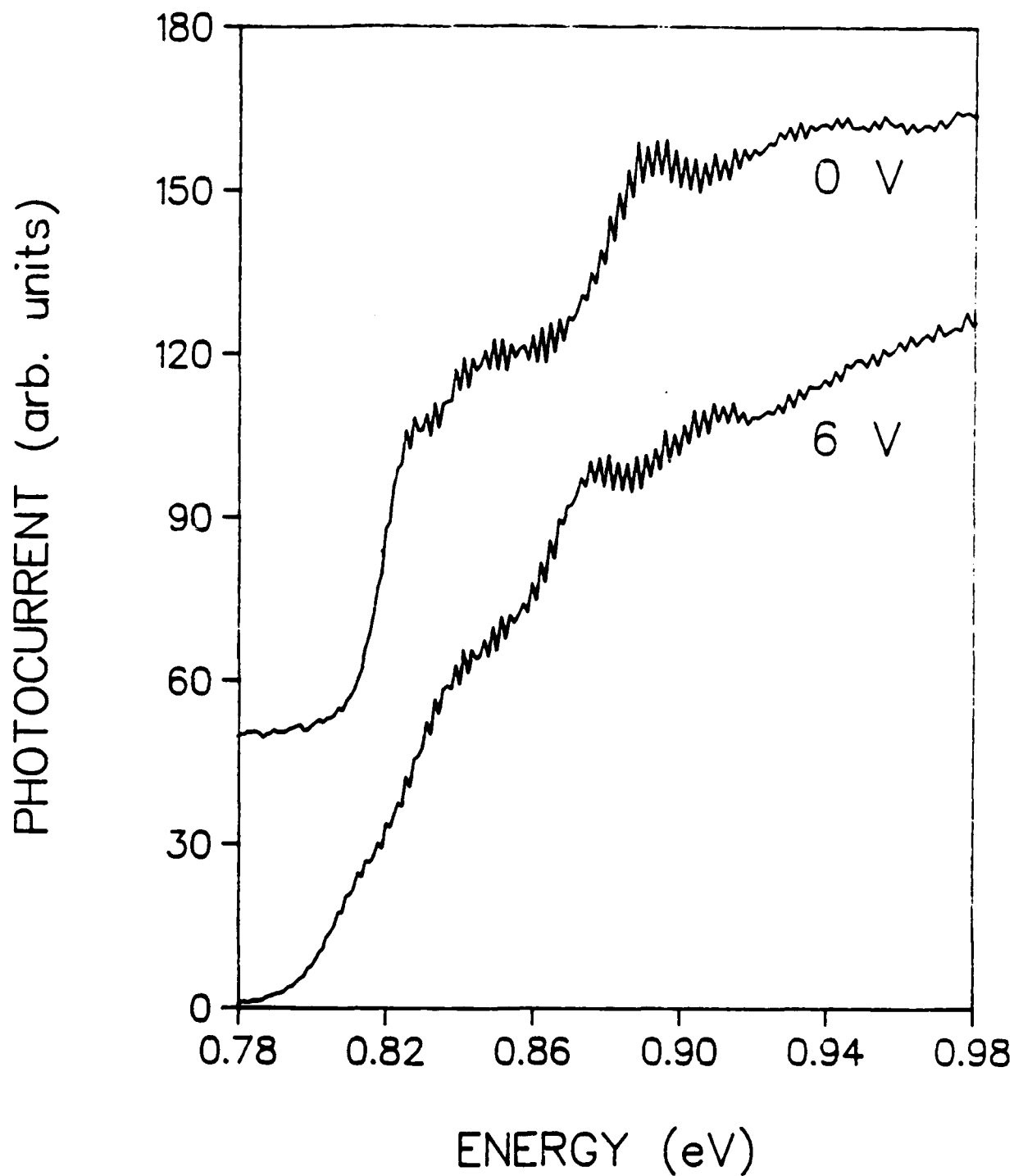


FIG. 23. Room-temperature photocurrent spectra of an InGaAs/InAlAs MQW waveguide sample (EO-75) containing 7.5- and 5.0-nm quantum wells coupled by a 1.6-nm barrier at 0 V and 6 V reverse bias.

not resolved in our previous photocurrent samples because those samples were much thicker.

The quantum-well waveguides were measured and analyzed as described in Section III.C, and the results of phase-shift and transmission measurements made on each of the samples are shown in Fig. 24. In the upper plot (a) optical phase shifts (TM polarization) of the two samples as a function of applied bias (measured in our Mach-Zehnder interferometer using an infrared He-Ne laser with a wavelength of  $1.523 \mu\text{m}$ ) are compared. The dashed lines represent errors as determined by repeating the measurements on different days or after realigning the sample in the interferometer. At biases for which the waveguide regions were highly-absorbing, the measurements were unreliable due to interference between the guided light and light that traveled through the transparent substrate. The phase shifts measured in the coupled-well sample are considerably larger than those of the uncoupled-well sample throughout the range of applied biases, because of the effects of coupling on the field dependence of the absorption energies. Because the laser wavelength is very close to the absorption edges of the samples, there is a substantial amount of absorption at zero bias. The transmission through the ACQW sample decreases rapidly with bias, as shown in Fig. 24 (b), and therefore we were unable to observe the inter-well ( $l_1e_1$ ) exciton directly in our measurement. Nevertheless, the rapid decrease in transmission and large phase-shift observed in this sample can be associated with the inter-well transition. In Fig. 25, our phase shift and transmission results have been converted to changes in the real ( $\Delta n$ ) and imaginary ( $\Delta k$ ) parts of the effective refractive index of the waveguide.

Our results can be understood in terms of the two-subband model described in Section III.C. We have performed calculations of the electro-refraction expected from both the ACQW and uncoupled-well waveguides at wavelengths of 1.52, 1.56, and  $1.6 \mu\text{m}$ .

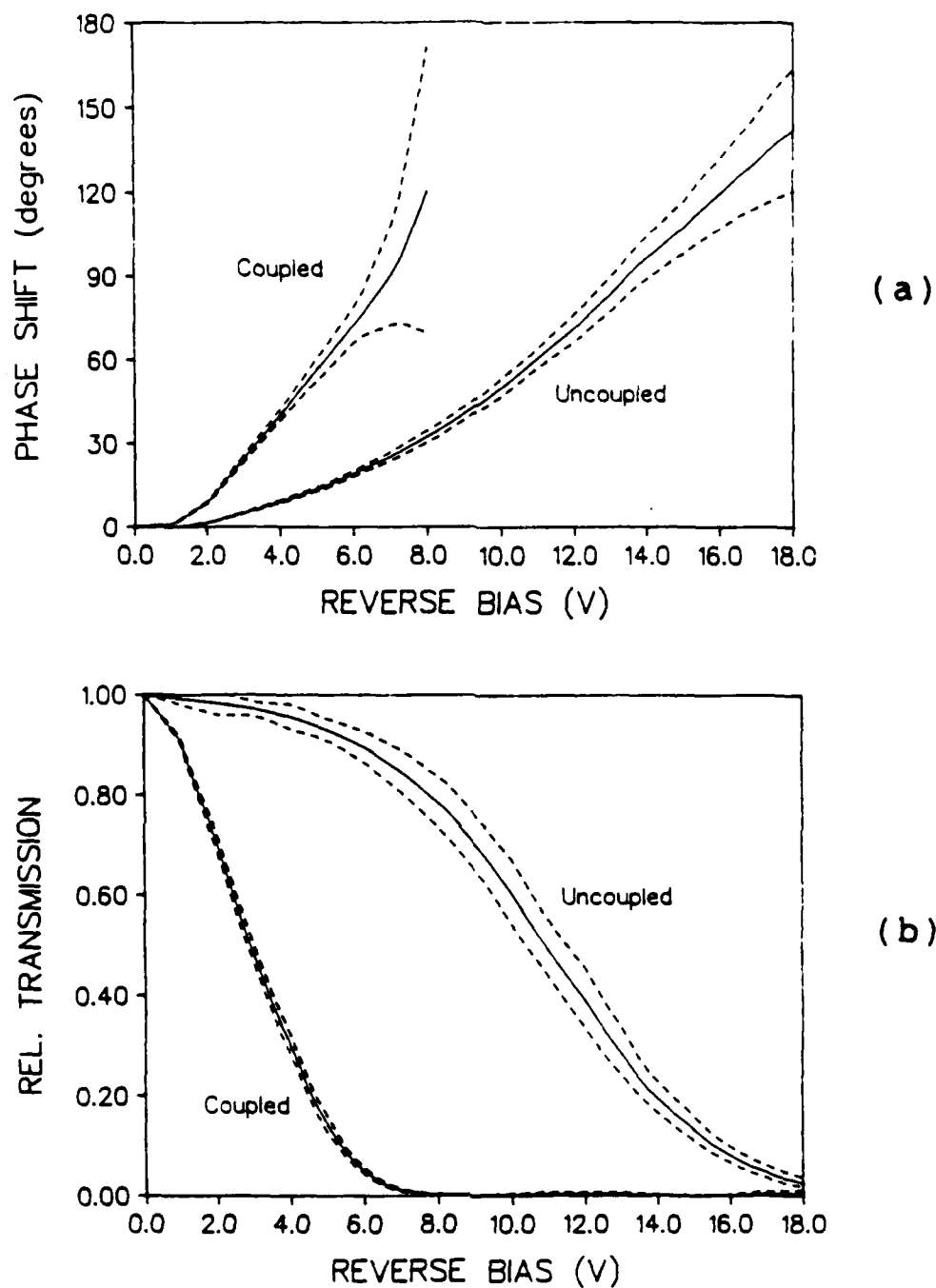


FIG. 24. Phase shift (a) and relative transmission (b) measured as a function of reverse bias in 250- $\mu\text{m}$ -long waveguides containing uncoupled wells (sample EO-77) and asymmetric coupled wells (sample EO-75) of InGaAs/InAlAs. Measurements were made using a Mach-Zehnder interferometer operated at a wavelength of 1.523  $\mu\text{m}$  in TM polarization. The coupled-well sample showed a much more rapid increase in the phase shift (and a corresponding decrease in the transmission) with increasing reverse bias due to the strongly shifting inter-well light-hole transition.

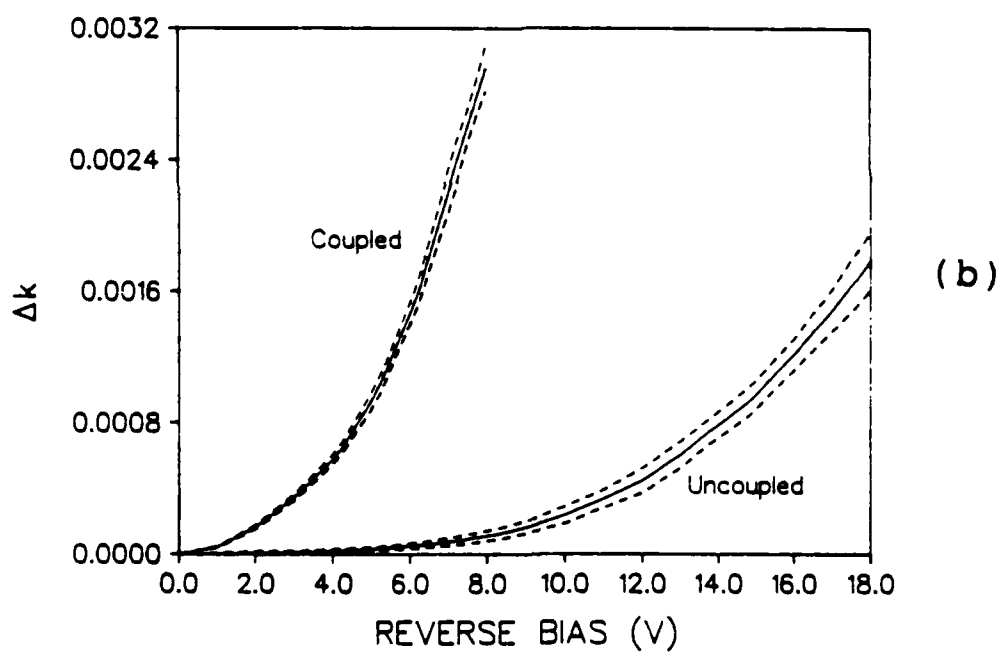
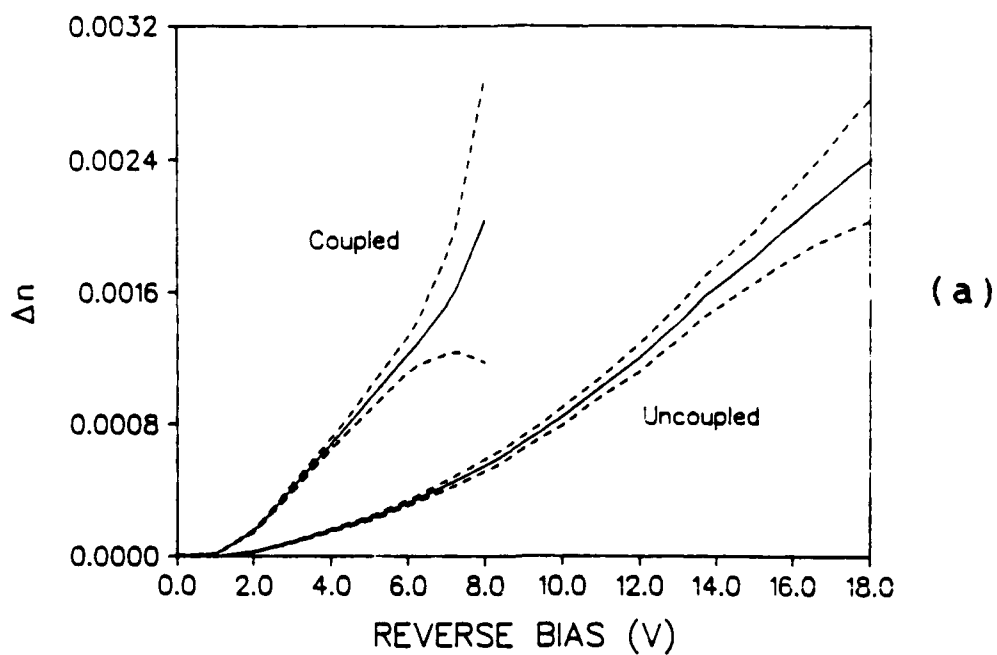


FIG. 25. Changes in the real (a) and imaginary (b) parts of the effective waveguide refractive index as a function of reverse bias at  $1.523 \mu\text{m}$  in TM polarization in  $250\text{-}\mu\text{m}$ -long waveguides containing uncoupled wells (sample EO-77) and asymmetric coupled wells (sample EO-75) of InGaAs/InAlAs.

Results of the calculations, shown in Fig. 26, confirm our interpretation of the experimental data and show the expected performance of the devices at the other wavelengths. As was the case for the GaAs ACQW waveguide described in Section III.C, a larger detuning from the exciton resonance should result in a more favorable value of the chirp parameter  $\Delta n/\Delta k$  for phase modulation. Excellent performance as an intensity modulator is obtained at 1.523  $\mu\text{m}$ , where the measurements were made. At this wavelength the chirp parameter is nearly 1 over a wide range of biases. In our measurements, we observed 20:1 modulation at about 6.5-V reverse bias, with a corresponding phase shift of about 140 degrees.

Our results have shown that effective intensity and phase modulators can be obtained in the InGaAs/InAlAs material system grown on InP, in contrast with results reported previously by others.<sup>38,39</sup> We have also shown that use of the ACQW system allows additional degrees of freedom in design that permit the realization of structures with better modulation characteristics in the 1.55- $\mu\text{m}$  region relative to devices based on the QCSE<sup>5</sup> that occurs in uncoupled structures.



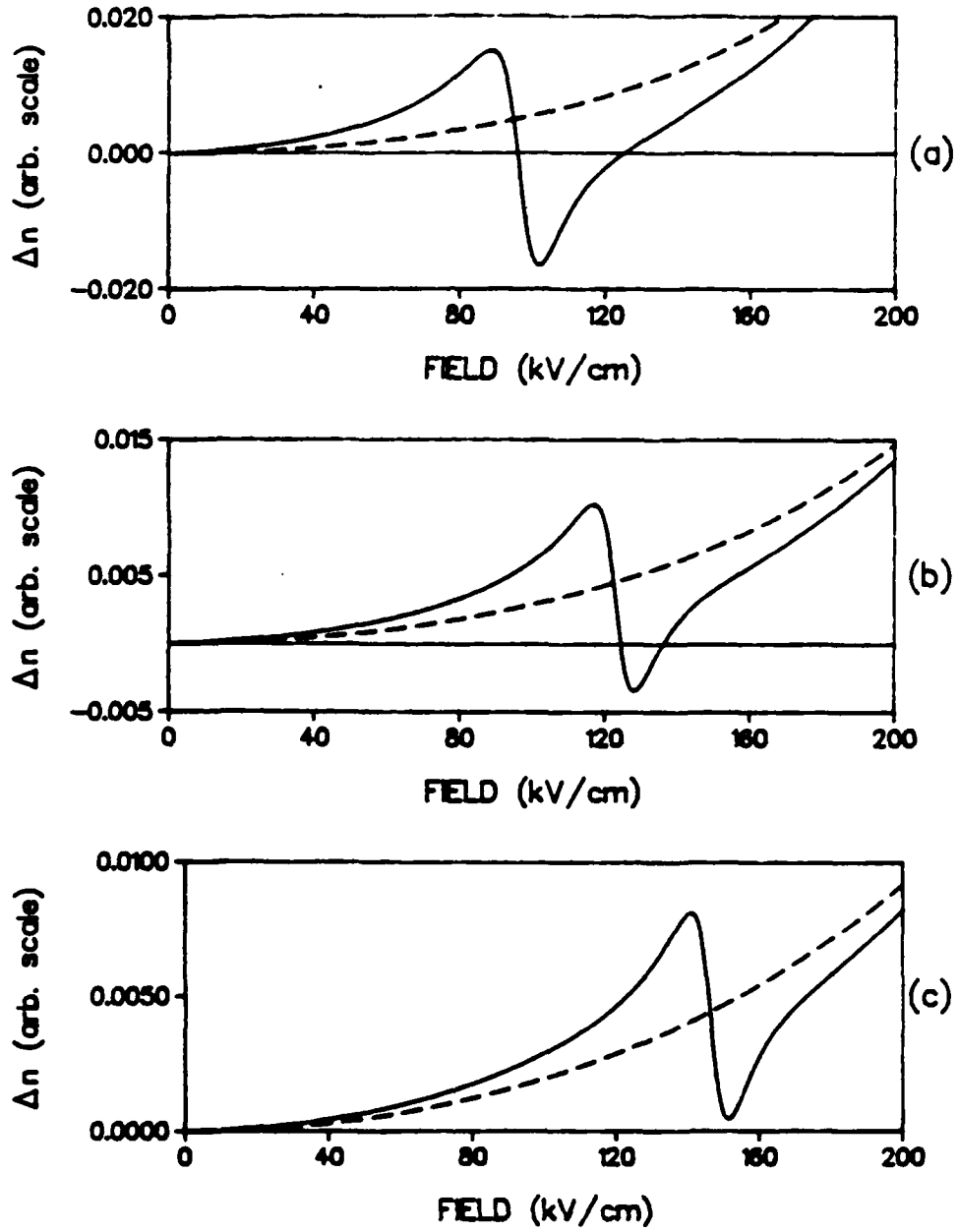


FIG. 26. Calculated changes in the real part of the MQW refractive index for the uncoupled and ACQW waveguides at wavelengths of (a) 1.52, (b) 1.56, and (c) 1.60  $\mu\text{m}$ . Calculations were performed assuming a light-hole exciton binding energy of 15 meV, an exciton half-width of 5 meV, and a minimum splitting  $\Delta = 27.6$  meV of the two electron states.

## V. DISCUSSION AND CONCLUSIONS

As a result of our in-depth studies of the coupling between electron subbands in ACQW structures, we have been able to design waveguide intensity and phase modulators in the InGaAs/InAlAs material system for operation in the 1.55- $\mu\text{m}$  wavelength region that have distinct advantages over modulators based on the QCSE. We have also shown that, in contrast with previous studies, it is possible to grow high-quality InGaAs/InAlAs quantum wells in waveguide structures and therefore to obtain modulation mechanisms in this material system that are in accord with theoretical expectations. For both reasons, the present study can be considered a success, and we expect that, with a reasonable amount of further development, the InGaAs/InAlAs ACQW waveguide modulators should play an important role in the development of future fiber-optic systems. Our results in the GaAs/AlGaAs system should also be important for practical application.

### A. SUMMARY OF THE CONTRACT RESULTS

When we first proposed our study of ACQWs, we suggested that enhanced phase modulation would result from a decrease in the integrated absorption of the excitons in the two wells as an applied bias brought the lowest electron subbands of the two wells into resonance. Detailed calculations of the exciton binding energies and the exciton oscillator strengths in a prototype GaAs/AlGaAs ACQW system (performed as part of the contract work) showed instead that the proposed effect was weak and should lead to a slight increase in the electro-refraction of ACQWs in comparison with uncoupled wells. In addition, in experimental studies, the first few GaAs/AlGaAs ACQW samples grown for the contract showed no evidence of resonant coupling of electron subbands and

exhibited unexpected nonlinear optical effects.

Finally, low-temperature photocurrent studies of later samples showed the effects of coupling unambiguously. In attempts to confirm our predictions using GaAs/AlGaAs ACQW waveguides, we noted resonances in the phase shifts (shown in Fig. 12) that were larger than we had anticipated based on the expected change in the integrated absorption. Also, we had not expected the bias at which the resonance occurred to depend on the probing wavelength. Detailed Kramers-Kronig calculations (described in Section III.C) made it clear to us that the observed effect was not associated with a decrease in the integrated absorption *at* resonance but rather was a direct consequence of the "forbidden" inter-well transition that occurs *beyond* the resonance of the two electron states and that dominates the below-bandgap optical properties of ACQWs. This effect was totally unexpected, although it would have been quite obvious had we performed the theoretical calculation first. In fact, the effect that we observed is much stronger in many instances than the one we had originally proposed.

Having found a desirable effect and having achieved a detailed understanding of its origin, it was then relatively simple for us to exploit it by designing samples in the InGaAs/InAlAs system wherein the effect would be quite strong and its advantages over the QCSE would be apparent. We spent a considerable amount of effort (some of it supported by internal funds) to optimize the quality of InGaAs and InAlAs layers grown by MBE, so that the desired phenomena would not be obscured by poor quality of the MQW samples. Once a good sample design was obtained and good material was being grown on the MBE, we grew some relatively thick MQW samples to verify that we could grow good MQW structures. Our room-temperature photocurrent studies on these samples showed that the phenomena observed originally in the GaAs/AlGaAs system could be repeated (and substantially enhanced by slight design changes) in the InGaAs/InAlAs system.

Details of the level crossings and resonance phenomena were confirmed by comparing results of low-temperature photocurrent studies with the theoretical calculations. Waveguides grown with the same quantum-well structures as the thicker samples exhibited the expected phase- and intensity-modulation behavior and showed many of the advantages of the ACQW system over uncoupled-well systems.

## B. ADVANTAGES OF COUPLED QUANTUM WELLS

The principal advantage of the ACQW system over conventional uncoupled-well modulators based on the QCSE is that it provides more degrees of freedom for designing optimized structures. In structures having uncoupled, equal-sized wells, the only degrees of freedom are the width of the well and the total number of wells. In many applications, these are predetermined by the system requirements, and there are no degrees of freedom left with which to optimize the design of the modulator. For example, in fiber-optics applications, it is desirable to have modulators that operate at either 1.3 or 1.55  $\mu\text{m}$ . The width of a quantum well for a QCSE modulator is then constrained to be on the order of 3 nm for 1.3  $\mu\text{m}$  or 7 nm for 1.55  $\mu\text{m}$ . For wells this thin, the QCSE is weak, and large reverse biases must be applied to the modulator in order to obtain sufficient phase shift and/or modulation depth. Furthermore, although many of the studies of phase and intensity modulation reported in the literature have used multi-mode waveguide samples containing many quantum wells, in reality the military applications of interest may require single-mode waveguides, which must contain only a few wells to limit the overall thickness of the core region.

The ACQW system has a sufficient number of degrees of freedom to overcome these limitations. The size of the effects due to the inter-well transition in these structures does not depend substantially on the width of the larger well, and this parameter may be

chosen to give maximum performance of the modulator *at the wavelength of interest*. Our results have been obtained in single-mode guides, and we have shown that substantial effects may be observed without resorting to multi-mode structures. In addition to the width of the widest well and the number of wells, the thickness of the tunnel barrier and the width of the smaller well can be varied to optimize the performance. It is expected that, with these additional parameters, structures that show vastly improved performance over QCSE devices can be designed to operate in any wavelength region that is accessible with quantum-well devices.

### C. DESIGN OF OPTIMIZED ACQW STRUCTURES

The greatest advantage of ACQW modulators over QCSE modulators is achieved when the coupling between electron subbands of the two wells is strong. Since the strength of coupling varies as  $\exp[-\gamma b]$ , where  $b$  is the thickness of the tunneling barrier separating the two wells, it is obvious that  $b$  should be small (on the order of 1-2 nm). However, if  $b$  is less than about 1 nm, the electron subbands are strongly coupled even at zero bias, and therefore the optical properties do not change rapidly with applied bias.

The bias at which resonance occurs is given approximately by

$$V_r = 2d\Delta E/(a_1 + a_2 + 2b) - V_{bi} \quad , \quad (9)$$

where  $d$  is the thickness of the intrinsic region of the diode,  $\Delta E$  is the energy separation of the electron subbands of the two (uncoupled) wells at zero field, and  $V_{bi}$  is the built-in potential of the diode. The largest change in the refractive index of the ACQW system occurs between zero bias and just past the resonance bias, so it is important to keep  $V_r$  as small as possible consistent with a large change in the optical properties. In our studies,  $d$  was kept relatively large so we could resolve expected features in the electro-absorption

and electro-refraction. However, to maximize the phase shift (or modulation) per volt applied to the sample,  $d$  could be made as thin as the waveguide core region (i.e., on the order of 200 nm), in which case the modulators could operate effectively with biases on the order of 1-2 V.

The best modulation characteristics are obtained when the relative well widths and the barrier thickness are chosen so that the wells are essentially uncoupled at zero bias but begin to couple when a small reverse bias is applied. This condition implies that the width of the smaller well,  $a_2$ , is not too different from the width of the larger well,  $a_1$ . This is because the quantity  $\Delta E$  in Eq. (9) is zero when  $a_1 = a_2$ ; thus, making  $a_2$  nearly equal to  $a_1$  keeps this quantity (and therefore  $V_r$ ) small. However, the bias range over which coupling between the wells is strong is proportional to  $\exp[-\gamma b]$ , so some difference between the well widths must be retained or, again, the system will behave like a symmetric system, and the advantages of the ACQW approach will be lost. Although we have not performed a detailed design study covering all reasonable ranges in the parameters, we believe that the design of the InGaAs/InAlAs modulator discussed in Section IV.C (7.5- and 5.0-nm wells, 1.6- nm barrier) is close to optimum for operation in the 1.55- $\mu\text{m}$  range.

The thickness of the larger quantum well should be chosen such that the absorption edge appropriate for the chosen polarization (in our case, the  $l_1e_1$  exciton absorption edge) is just above the photon energy for intensity modulators and somewhat ( $\sim 50$ -100 meV) above the photon energy for phase modulators. We used TM-polarized light exclusively in our work to eliminate heavy-hole transitions and thereby simplify the task of interpreting the results. In practical applications, it may be advantageous to use TE polarization instead, since the heavy-hole states are more easily polarizable by an applied bias, and somewhat larger effects should be observable. If TE-polarized light is used, the

wells must be narrower ( $\sim 6$  nm) so that the heavy-hole exciton absorption occurs at about  $1.48 \mu\text{m}$ .

#### D. RECOMMENDATIONS FOR FURTHER STUDY

The present research has demonstrated that ACQW systems have advantages over other quantum-well systems for use as intensity and phase modulators. There are several areas in which further research and development would be warranted:

- (a) Measurements of electro-absorption and electro-refraction of the present InGaAs/InAlAs ACQW waveguides with a tunable laser, such as a NaCl color center laser. This would permit a more thorough test of the electro-refraction model and would give additional insight into the design of optimized devices for operation at  $1.55 \mu\text{m}$ .
- (b) Measurements of the waveguide samples grown for the contract with TE-polarized light. We avoided this, because we believed that the additional heavy-hole transitions would complicate the interpretation of the results. However, the modulators might work better with TE polarization, as mentioned above. Optimization of structures for TE polarization would require design and growth of additional samples.
- (c) Design studies to determine optimum ACQW geometries for various applications. These would quantify the conclusions of Section V.C above.
- (d) Studies of hole-state coupling effects. The present contract concentrated exclusively on electron subband resonances, mainly (again) for ease in interpreting the data. By growing samples in which the ordering of the wide and narrow wells is reversed, one can bring the hole subbands into resonance by applying a reverse bias. This would yield some new effects, since the light-hole subbands would be strongly affected by

the coupling but the heavy-hole subbands would be nearly unaffected. It is possible that yet stronger effects would be observed in this geometry.

- (e) Examination of the potential of the ACQW geometry for optical controllability. If the ACQW system is biased beyond resonance, optically-created electron-hole pairs become spatially separated, with the electrons tunneling into the narrow well and the holes remaining behind in the wide well. The recombination process is inhibited, and a macroscopic space-charge builds up that tends to cancel the applied bias. Thus, an above-bandgap light signal, rather than an applied bias, can be used to modulate below-bandgap light. (This phenomenon is similar to that observed in sample 259, but would occur at higher light intensities in good-quality samples.)
- (f) Fabrication of ACQW waveguides that confine light to a single mode in two dimensions, i.e., rib or ridge waveguides, by wet chemical etching or reactive-ion etching. These would have to be anti-reflection coated to minimize Fabry-Perot oscillations in phase-modulation structures. Waveguides of this type are required for many applications, including on-chip integration with lasers.

In conclusion, we have demonstrated that the ACQW system can be used effectively in phase and intensity modulators appropriate for the 1.55- $\mu\text{m}$  wavelength band appropriate for application in fiber-optic systems.



## ACKNOWLEDGMENTS

Responsibility for operation of the Labs' Physical Electronics PHI-425B MBE machine originally rested with Rick Wilson (now at the University of Maryland, Laboratory for Physical Sciences) and later with Doug Martel and Dave Gill; these individuals grew all the GaAs/AlGaAs quantum-well samples for this contract, and DG was responsible for much of the early work on InGaAs growth on the PHI MBE. The InGaAs/InAlAs MQW samples were all grown on the Labs' Varian GEN-II MBE by one of us (RPL), with the assistance of Fred Towner. Processing of the GaAs/AlGaAs samples was performed by Jeff Whisnant and one of us (JWL), and of the InGaAs/InAlAs samples by Scott Horst. Transmission, photocurrent, and (earlier) reflectivity measurements were performed entirely by JWL. Dr. Kirk Steijn (now at Dupont Corp.) set up the Mach-Zehnder interferometer, performed the initial phase- and intensity-modulation measurements in the waveguides, and was primarily responsible for measuring the GaAs/AlGaAs waveguides. Dr. Ken Ritter refined the experimental setup and measured the electro-optic properties of the InGaAs/InAlAs waveguides. RPL performed all theoretical calculations (usually after much discussion and input from JWL).

Although they did not contribute directly to the contract, it is appropriate to acknowledge the assistance of several individuals in the general area of quantum-well physics. We have benefitted from a long-term collaboration with Ben Shanabrook, Orest Glembocki, and Eric Snow at Naval Research Laboratory, whose in-depth knowledge of quantum wells (and semiconductor physics in general) was helpful to us at many stages during the contract and who have continued to express interest in the ACQW system and in our results. Y. J. (Ray) Chen (formerly at GTE Laboratory and now at University of Maryland, Baltimore County), who had done some work in symmetric coupled-well systems while at GTE, showed great interest in our work and made his expertise available to us on

many occasions. Shlomo Ovadia (formerly a post-doc at University of Maryland, College Park, and now at IBM Corp.) and Chi Lee (UMCP) collaborated with us on our photo-current studies of nonuniform fields in quantum wells. At Martin Marietta Laboratories, Parvez Uppal made available to us his considerable expertise in MBE growth in many fruitful discussions, particularly concerning growth of InGaAs on InP. Finally, Frank Crowne participated in several discussions on the theory of III-V band structures and energy-level calculations in quantum wells.

## REFERENCES

- <sup>1</sup>D. A. B. Miller, D. S. Chemla, T. C. Damen, A. C. Gossard, W. Wiegmann, T. H. Wood, and C. A. Burrus, *Phys. Rev. B* **32**, 1043 (1985).
- <sup>2</sup>D. A. B. Miller, D. S. Chemla, T. C. Damen, A. C. Gossard, W. Wiegmann, T. H. Wood, and C. A. Burrus, *Phys. Rev. Lett.* **53**, 2173 (1984).
- <sup>3</sup>J. W. Little and R. P. Leavitt, "Feasibility study of resonant tunneling electro-optic quantum-well devices," Martin Marietta Laboratories Technical Report 87-76 (mid-term contract report).
- <sup>4</sup>F. Stern, in *Solid State Physics*, ed. by F. Seitz and D. Turnbull (Academic, New York, 1963), Vol. 5, p. 299.
- <sup>5</sup>J. S. Weiner, D. A. B. Miller, and D. S. Chemla, *Appl. Phys. Lett.* **50**, 842 (1987).
- <sup>6</sup>G. Bastard, *Phys. Rev. B* **24**, 5693 (1981).
- <sup>7</sup>U. Rossler, *Solid State Commun.* **49**, 943 (1984).
- <sup>8</sup>J. N. Schulman and Y.-C. Chang, *Phys. Rev. B* **31**, 2056 (1985).
- <sup>9</sup>J. W. Little, J. K. Whisnant, R. P. Leavitt, and R. A. Wilson, *Appl. Phys. Lett.* **51**, 1786 (1987).
- <sup>10</sup>R. T. Collins, K. von Klitzing, and K. Ploog, *Phys. Rev. B* **33**, 4378 (1986).
- <sup>11</sup>M. Whitehead, G. Parry, K. Woodbridge, P. J. Dobson, and G. Duggan, *Appl. Phys. Lett.* **52**, 345 (1988).
- <sup>12</sup>J. W. Little, R. P. Leavitt, S. Ovadia, and C. H. Lee, *Appl. Phys. Lett.* (to be published).

- <sup>13</sup>D. J. Newson and A. Kurobe, *Electron. Lett.* **23**, 439 (1987).
- <sup>14</sup>S. M. Sze, *Physics of Semiconductor Devices* (Wiley, New York, 1981), pp. 74 ff.
- <sup>15</sup>K. K. Choi, C. G. Bethea, J. Walker, and R. J. Malik, *Appl. Phys. Lett.* **52**, 1979 (1988).
- <sup>16</sup>M. Ilegems, in *The Technology and Physics of Molecular Beam Epitaxy*, ed. by E. H. C. Parker (Plenum, New York, 1985), p. 100.
- <sup>17</sup>E. J. Austin and M. Jaros, *J. Phys.* **C19**, 533 (1986).
- <sup>18</sup>J. Khurgin, *Appl. Phys. Lett.* **51**, 2100 (1987).
- <sup>19</sup>C. Delalande, U. O. Ziemelis, G. Bastard, M. Voos, A. C. Gossard, and W. Wiegmann, *Surf. Sci.* **142**, 498 (1984).
- <sup>20</sup>M. N. Islam, R. L. Hillman, D. A. B. Miller, D. S. Chemla, A. C. Gossard, and J. H. English, *Appl. Phys. Lett.* **50**, 1098 (1987).
- <sup>21</sup>Y. J. Chen, E. S. Koteles, B. S. Elman, and C. A. Armiento, *Phys. Rev.* **B36**, 4562 (1987).
- <sup>22</sup>H. Q. Le, J. J. Zayhowski, and W. D. Goodhue, *Appl. Phys. Lett.* **50**, 1518 (1987).
- <sup>23</sup>J. W. Little and R. P. Leavitt, *Phys. Rev. B* **39**, 1365 (1989).
- <sup>24</sup>R. Dingle, in *Festkörperprobleme: Advances in Solid State Physics*, edited by H. J. Queisser (Pergamon-Vieweg, Braunschweig, 1975), Vol. 15, p. 21.
- <sup>25</sup>R. C. Miller, A. C. Gossard, D. A. Kleinman, and O. Munteanu, *Phys. Rev.* **B29**, 3740 (1984).
- <sup>26</sup>R. C. Miller, A. C. Gossard, and D. A. Kleinman, *Phys. Rev.* **B32**, 5443 (1985).

- <sup>27</sup>H. Kroemer, *Surf. Sci.* **174**, 299 (1986).
- <sup>28</sup>M. Glick, F. K. Reinhart, G. Weimann, and W. Schlapp, *Helv. Phys. Acta* **59**, 137 (1986).
- <sup>29</sup>M. Glick, F. K. Reinhart, G. Weimann, and W. Schlapp, *Appl. Phys. Lett.* **48**, 989 (1986).
- <sup>30</sup>T. H. Wood, R. W. Tkach, and A. R. Chraplyvy, *Appl. Phys. Lett.* **50**, 798 (1987).
- <sup>31</sup>J. E. Zucker, T. L. Henderson, and C. A. Burrus, *Appl. Phys. Lett.* **52**, 945 (1988).
- <sup>32</sup>K. W. Steijn, R. P. Leavitt, and J. W. Little, *Appl. Phys. Lett.* (to be published).
- <sup>33</sup>P. Ruden and G. H. Dohler, *Phys. Rev. B* **27**, 3538 (1983).
- <sup>34</sup>J. D. Grange, in Ref. 16, p. 56.
- <sup>35</sup>S. Nojima, K. Nakashima, Y. Kawamura, and H. Asahi, *J. Appl. Phys.* **63**, 2795 (1988).
- <sup>36</sup>J. W. Little, R. P. Leavitt, and S. Horst, *Phys. Rev. B* (to be published).
- <sup>37</sup>E. J. Austin and M. Jaros, *Phys. Rev. B* **37**, 9087 (1985).
- <sup>38</sup>K. Wakita, Y. Kawamura, Y. Yoshikuni, H. Asahi, and S. Uehara, *IEEE J. Quantum Electron.* **QE-22**, 1831 (1986).
- <sup>39</sup>K. Wakita, Y. Yoshikuni, and Y. Kawamura, *Electron. Lett.* **23**, 303 (1987).
- <sup>40</sup>U. Koren, T. L. Koch, H. Presting, and B. I. Miller, *Appl. Phys. Lett.* **50**, 368 (1987).
- <sup>41</sup>J. E. Zucker, I. Bar-Joseph, G. Sucha, U. Koren, B. I. Miller, and D. S. Chemla, *Electron. Lett.* **24**, 458 (1988).

<sup>42</sup>K. J. Ritter, R. P. Leavitt, J. W. Little, K. W. Steijn, and S. C. Horst, Appl. Phys. Lett.  
(manuscript in preparation).

## APPENDIX A. DESCRIPTION OF SAMPLES

### GaAs/AlGaAs (grown on PHI 425B MBE machine)

number	n	a1	a2	b1	b2	d	Sec.	Comments
259	40	8.0	4.0	5.0	10.0	1.4	II.B	Transmission
351	40	8.5	4.3	0.8	10.0	1.0	II.B	Transmission
800	40	7.2	...	...	9.8	0.98	III.A	Photocurrent**
802	40	8.8	3.6	9.0	9.8	1.55	III.A	Photocurrent
919*	7	8.5	4.3	2.1	8.5	1.5	III.C	Waveguide
1121*	7	9.5	4.5	2.4	9.8	1.5	III.B	Photocurrent

### InGaAs/InAlAs (grown on Varian GEN-II MBE machine)

number	n	a1	a2	b1	b2	d	Sec.	Comments
EO-64*	40	7.5	...	...	10.0	1.0	IV.B	Photocurrent
EO-72*	29	7.5	5.0	1.6	10.0	1.0	IV.B	Photocurrent
EO-74	13	7.5	5.0	1.6	10.0	1.0	...	None
EO-75*	13	7.5	5.0	1.6	10.0	1.0	IV.C	Waveguide
EO-76	13	7.5	5.0	1.6	10.0	1.0	...	None
EO-77*	13	7.5	...	...	16.6	1.0	IV.C	Waveguide
EO-79***	13	7.5	5.0	1.6	10.0	1.0	IV.D	None

#### NOTATION:

- number - identifying sample number.
- n - number of MQW periods
- a1 - width of wide quantum well
- a2 - width of narrow quantum well
- b1 - width of coupling barrier
- b2 - width of barrier separating well pairs
- d - total intrinsic region thickness
- Sec. - Section of this report in which sample is discussed

#### COMMENTS:

- Transmission - sample was characterized with room-temperature transmission measurements.
- Photocurrent - sample was characterized with room- (and possibly low-) temperature photocurrent measurements.
- Waveguide - sample was processed into slab waveguides and characterized with electro-absorption and electro-refraction measurements in a Mach-Zehnder interferometer.
- None - Sample was processed into an appropriate device but no measurements were made other than room-temperature transmission at zero bias. These samples are available for further study by RADC if desired.

\*Will be delivered as part of the contract.

\*\*Sample containing only a single well width.

\*\*\*Sample EO-79 has InAlAs waveguide cladding regions; all other InGaAs/InAlAs waveguides have InGaAs/InAlAs superlattice cladding.

## APPENDIX B. EXTERNAL PUBLICATIONS AND PRESENTATIONS RESULTING FROM THE CONTRACT

1. J. W. Little, J. K. Whisnant, R. P. Leavitt, and R. A. Wilson, "Extremely low-intensity optical nonlinearities in asymmetric coupled quantum wells," Appl. Phys. Lett. **51**, 1786 (1987).
2. J. W. Little and R. P. Leavitt, "Low-temperature photocurrent spectroscopy of asymmetric coupled-quantum-well structures," Phys. Rev. B **39**, 1365 (1989).
3. J. W. Little, R. P. Leavitt, S. Ovadia, and C. H. Lee, "Optical characterization of nonuniform electric fields in multiple-quantum-well diodes," Appl. Phys. Lett. (to be published). (Work was not performed for the contract but is closely related.)
4. K. W. Steijn, R. P. Leavitt, and J. W. Little, "Electro-absorption and electro-refraction in GaAs/AlGaAs waveguides containing asymmetric coupled quantum wells," Appl. Phys. Lett. (to be published).
5. J. W. Little, R. P. Leavitt, and S. Horst, Appl. Phys. Lett., "Electro-absorption in InGaAs/InAlAs asymmetric coupled quantum wells grown on InP substrates," Phys. Rev. B, Brief Reports (to be published).
6. K. J. Ritter, R. P. Leavitt, J. W. Little, K. W. Steijn, and S. C. Horst, "Electro-absorption and electro-refraction in InGaAs/InAlAs asymmetric coupled-quantum-well waveguides," Appl. Phys. Lett. (manuscript in preparation).
7. J. W. Little, J. K. Whisnant, R. P. Leavitt, and R. A. Wilson, "Optical nonlinearities at low light intensities in asymmetric coupled quantum well structures," March 1987 meeting of the American Physical Society.



8. R. P. Leavitt and J. W. Little, "Exciton binding energies and optical absorption in asymmetric coupled quantum well structures," March 1987 meeting of the American Physical Society.
9. J. W. Little, J. K. Whisnant, R. P. Leavitt, and R. A. Wilson, "Optical nonlinearities at low light intensities in asymmetric coupled quantum well structures," April 1987 International Quantum Electronics Conference.
10. J. W. Little, K. W. Steijn, J. K. Whisnant, and R. P. Leavitt, "Low-temperature photocurrent in asymmetric coupled quantum well diodes," March 1988 meeting of the American Physical Society.
11. K. W. Steijn, J. W. Little, and R. P. Leavitt, "Electro-refraction in asymmetric coupled quantum well waveguides," March 1988 conference on Integrated and Guided Wave Optics.
12. J. W. Little, K. J. Ritter, R. P. Leavitt, and S. C. Horst, "Photocurrent studies of electron state coupling in InGaAs/InAlAs asymmetric coupled quantum wells grown on InP substrates," March 1989 meeting of the American Physical Society.
13. K. J. Ritter, R. P. Leavitt, J. W. Little, and K. W. Steijn, "Electro-absorption and electro-refraction in asymmetric coupled quantum well waveguides," March 1989 meeting of the American Physical Society.
14. R. P. Leavitt, K. J. Ritter, J. W. Little, S. C. Horst, and K. W. Steijn, "Electro-absorption and electro-refraction in InGaAs/InAlAs waveguides containing asymmetric coupled quantum wells," April 1989 Conference on Quantum Electronics and Laser Science.



## *MISSION of Rome Air Development Center*

*RADC plans and executes research, development, test and selected acquisition programs in support of Command, Control, Communications and Intelligence (C<sup>3</sup>I) activities. Technical and engineering support within areas of competence is provided to ESD Program Offices (POs) and other ESD elements to perform effective acquisition of C<sup>3</sup>I systems. The areas of technical competence include communications, command and control, battle management information processing, surveillance sensors, intelligence data collection and handling, solid state sciences, electromagnetics, and propagation, and electronic reliability/maintainability and compatibility.*